

1 **Loss of CTRP10 results in female obesity with preserved metabolic health**

2
3 Fangluo Chen^{1,2}, Dylan C. Sarver^{1,2}, Muzna Saqib^{1,2}, Leandro M Velez^{3,4}, Susan Aja^{2,5}, Marcus M. Seldin^{3,4},
4 G. William Wong^{1,2}

5
6
7 Affiliations:

8 ¹Department of Physiology, Johns Hopkins University School of Medicine, Baltimore, Maryland, USA

9 ²Center for Metabolism and Obesity Research, Johns Hopkins University School of Medicine, Baltimore,
10 Maryland, USA

11 ³Department of Biological Chemistry, University of California, Irvine, Irvine, USA

12 ⁴Center for Epigenetics and Metabolism, University of California Irvine, Irvine, USA

13 ⁵Department of Neuroscience, Johns Hopkins University School of Medicine, Baltimore, Maryland, USA

14
15
16
17
18
19 Running head: CTRP10 deficiency uncouples obesity from metabolic dysfunction

20
21
22
23 Corresponding author: G. William Wong, E-mail: gwong@jhmi.edu, Department of Physiology, Johns Hopkins
24 University School of Medicine, Baltimore, MD 21205

25 Tel: 410-502-4862

26 Fax: 410-614-8033

29 **ABBREVIATIONS**

30

31	CTRP	C1q/TNF-related protein
32	DEG	Differentially expressed gene
33	EE	energy expenditure
34	gWAT	gonadal white adipose tissue
35	iWAT	inguinal white adipose tissue
36	HDL	High density lipoprotein
37	HFD	high-fat diet
38	i.p.	intraperitoneally
39	KO	knockout
40	LFD	low-fat diet
41	MHO	Metabolically healthy obese
42	NEFA	non-esterified free fatty acids
43	RER	respiratory exchange ratio
44	TG	triglyceride
45	VLDL	Very low density lipoprotein
46	WT	wildtype

47

48

49

50

51

52

53

54

55

56

57 **ABSTRACT**

58

59 Obesity is a major risk factor for type 2 diabetes, dyslipidemia, cardiovascular disease, and hypertension.
60 Intriguingly, there is a subset of metabolically healthy obese (MHO) individuals who are seemingly able to
61 maintain a healthy metabolic profile free of metabolic syndrome. The molecular underpinnings of MHO, however,
62 are not well understood. Here, we report that CTRP10/C1QL2-deficient mice represent a unique female model of
63 MHO. CTRP10 modulates weight gain in a striking and sexually dimorphic manner. Female, but not male, mice
64 lacking CTRP10 develop obesity with age on a low-fat diet while maintaining an otherwise healthy metabolic
65 profile. When fed an obesogenic diet, female *Ctrp10* knockout (KO) mice show rapid weight gain. Despite
66 pronounced obesity, *Ctrp10* KO female mice do not develop steatosis, dyslipidemia, glucose intolerance, insulin
67 resistance, oxidative stress, or low-grade inflammation. Obesity is largely uncoupled from metabolic dysregulation
68 in female KO mice. Multi-tissue transcriptomic analyses highlighted gene expression changes and pathways
69 associated with insulin-sensitive obesity. Transcriptional correlation of the differentially expressed gene (DEG)
70 orthologous in humans also show sex differences in gene connectivity within and across metabolic tissues,
71 underscoring the conserved sex-dependent function of CTRP10. Collectively, our findings suggest that CTRP10
72 negatively regulates body weight in females, and that loss of CTRP10 results in benign obesity with largely
73 preserved insulin sensitivity and metabolic health. This female MHO mouse model is valuable for understanding
74 sex-biased mechanisms that uncouple obesity from metabolic dysfunction.

75

76

77

78 Key words: Metabolism, Obesity, Diabetes, Metabolically healthy obese (MHO)

79

80

81

82

83

84

85 INTRODUCTION

86

87 The prevalence of obesity has nearly tripled in the past four decades and the underlying cause is complex and
88 multifactorial (1, 2). Genetics, environmental and social factors, and demographics all play a contributing role in
89 contributing to excessive weight gain in the setting of overnutrition (3, 4). Although obesity is a major risk factor
90 for type 2 diabetes, dyslipidemia, cardiovascular disease, and hypertension, not all obese individuals develop the
91 metabolic syndrome (5). There is a subset of metabolically healthy obese (MHO) individuals with an apparently
92 healthy metabolic profile free of some or most components of the metabolic syndrome (6, 7). The molecular and
93 physiological underpinnings of MHO are, however, not well understood. Novel preclinical animal models that can
94 recapitulate features of MHO will be valuable in illuminating pathways that resist the deleterious effects of obesity
95 and provide new therapeutic avenues to mitigate obesity-linked comorbidities.

96

97 The mechanisms that normally maintain body weight and metabolic homeostasis are complex and involve both cell
98 autonomous and non-cell autonomous mechanisms. Tissue crosstalk mediated by paracrine and endocrine factors
99 plays an especially important role in coordinating metabolic processes across organ systems to maintain energy
100 balance (8). Of the secretory proteins that circulate in plasma, C1q/TNF-related proteins (CTRP1-15) have emerged
101 as important regulators of insulin sensitivity, and glucose and lipid metabolism (9). We originally identified the first
102 seven members of the CTRP family based on shared sequence homology to the insulin-sensitizing adipokine,
103 adiponectin (10), and subsequently characterized additional members (11-16). All fifteen CTRPs share a common
104 C-terminal globular C1q domain and are part of the much larger C1q family (17, 18). The use of gain- and loss-of-
105 function mouse models has helped establish CTRP's role in controlling various aspects of sugar and fat metabolism
106 (12, 19-34). Additional diverse functions of CTRPs have also been demonstrated in the cardiovascular (35-47),
107 renal (48, 49), immune (20, 50, 51), sensory (52, 53), gastrointestinal (54), musculoskeletal (55-57), and the
108 nervous system (58-61).

109

110 Of the family members, CTRP10 (also known as C1QL2) is understudied and consequently only limited
111 information is available concerning its function. The best characterized role of CTRP10 is in the central nervous
112 system (CNS). It has been shown that CTRP10 secreted from mossy fibers is required for the proper clustering of

113 kainite-type glutamate receptors on postsynaptic CA3 pyramidal neurons in the hippocampus (62). It serves as a
114 transsynaptic organizer by directly binding to neurexin3 (Nrx3) on the presynaptic terminals, and to GluK2 and
115 GluK4 on the postsynaptic terminals (62). Additional putative roles of CTRP10 in the CNS have also been
116 suggested. Genome-wide association studies (GWAS) have implicated CTRP10/C1QL2 in cocaine use disorder
117 (63). In rat models of depression, *Ctrp10* expression is increased in the dentate gyrus and reduced in the nucleus
118 accumbens (64). In humans with a history of psychiatric disorders (e.g., schizophrenia), the expression of *CTRP10*
119 is elevated in the dorsolateral prefrontal cortex of both males and females (64). Whether and how CTRP10
120 contributes to addictive behavior and psychiatric disorders is unknown.

121

122 The potential function of CTRP10 in peripheral tissues, however, is essentially unknown and unexplored. The
123 present study was motivated by the well documented metabolic functions of many CTRP family members we have
124 characterized to date using genetic loss-of-function mouse models (19-28, 30, 31). We determined that the
125 expression of *Ctrp10* in peripheral tissues is modulated by diet and nutritional states, and thus may have a
126 metabolic role. We therefore used a genetic loss-of-function mouse model to determine if CTRP10 is required for
127 regulating systemic metabolism. We unexpectedly discovered a female-specific requirement of CTRP10 for body
128 weight control. We showed that the *Ctrp10* KO mice represent a unique female model of MHO with largely
129 preserved insulin sensitivity and metabolic health. This valuable mouse model can be used to inform sex-dependent
130 mechanisms that uncouple obesity from insulin resistance, dyslipidemia, and metabolic dysfunction.

131

132

133 **RESULTS**

134

135 **Nutritional regulation of *Ctrp10* expression in the brain and peripheral tissues**

136 CTRP10 protein is highly conserved from zebrafish to human (Fig. 1A), with amino acid identity of 67%, 71%,
137 77%, and 94% between the full-length human protein and the fish, frog, chicken, and mouse orthologs,
138 respectively. The conservation is much higher at the C-terminal globular C1q domain (93-100% identity) between
139 the orthologs. Among the 12 different mouse tissue examined, brain had the highest expression of *Ctrp10* (Fig. 1B),
140 consistent with previous findings (65). Expression of *Ctrp10* in peripheral tissues was variable and generally much

141 lower than in the brain (Fig. 1B). We first determined whether *Ctrp10* expression is modulated by nutrition and
142 metabolic state. Male mice were subjected to fasting and refeeding. In the refed period after an overnight fast, we
143 observed a significant downregulation of *Ctrp10* in the visceral (gonadal) white adipose tissue (gWAT), liver,
144 skeletal muscle, kidney, cerebellum, cortex, and hypothalamus relative to the fasted state (Fig. 1C). Next, we
145 examined whether an obesogenic diet alters the expression of *Ctrp10*. Male mice fed a high-fat diet for 12 weeks
146 had a modest increase in *Ctrp10* expression in brown adipose tissue (BAT) and heart and decreased expression in
147 skeletal muscle relative to mice fed a control low-fat diet (LFD) (Fig. 1D). These data indicate that *Ctrp10*
148 expression is dynamically regulated by acute alterations in energy balance, and perhaps to a lesser extent in
149 alterations to chronic nutritional state on an obesogenic diet.

150

151 **Generation of *Ctrp10* knockout (KO) mice**

152 We used mice lacking CTRP10 to address whether this secreted protein has a metabolic role in vivo. The mouse
153 *Ctrp10* gene consists of two exons (Fig. 1E). The CRISPR-Cas9 method was used to remove the entire protein
154 coding region spanning exon 1 and 2, thus ensuring a complete null allele (Fig. 1E-F). The targeted allele was
155 confirmed by sequencing. As expected, based on the gene deletion strategy, the *Ctrp10* transcript was absent from
156 KO mice (Fig. 1G).

157

158 **CTRP10 is largely dispensable for metabolic homeostasis in young mice fed a control low-fat diet**

159 The body weight and body composition of male mice fed a LFD were not different between genotypes (Fig. 2A-B).
160 By 20 weeks of age, female KO mice fed LFD had a modestly higher body weight relative to WT controls (Fig. 2
161 C), though the body composition was not different between genotypes (Fig. 2D). Food intake, physical activity, and
162 energy expenditure as measured by indirect calorimetry were also not different between genotypes of either sex
163 across the circadian cycle (light and dark) and metabolic states (*ad libitum* fed, fasted, refed) (Fig. 2E-J). Because
164 *Ctrp10* expression is regulated by nutritional states (Fig. 1C), we assessed serum metabolite levels in WT and KO
165 mice in response to fasting and refeeding. No significant differences in fasting and refeeding blood glucose, serum
166 insulin, triglyceride, cholesterol, non-esterified free fatty acids (NEFA), and β -hydroxybutyrate levels were
167 observed between genotypes of either sex, except the female KO mice had slightly lower fasting β -hydroxybutyrate
168 levels (Fig. 3A-B). We performed glucose and insulin tolerance tests to determine any potential differences in

169 glucose handling capacity and insulin sensitivity. No significant differences in glucose and insulin tolerance were
170 noted between genotypes of either sex (Fig. 3C-F). Together, these data indicate that CTRP10 is dispensable for
171 metabolic homeostasis when mice are young (< 20 weeks old) and fed a LFD.

172

173 **CTRP10-deficient female mice on a low-fat diet develop obesity with age**

174 Because female KO mice were slightly heavier at 20 weeks of age (Fig. 2C), we suspected the weight may diverge
175 further with age. Consequently, we monitored the body weight of female mice fed LFD over an extended period.
176 Indeed, the female KO mice gained significantly more weight and adiposity with age (Fig. 4A-C). Consistent with
177 greater adiposity, the adipocyte cell size (cross-sectional area) was also significantly larger in both gonadal
178 (visceral) white adipose tissue (gWAT) and inguinal (subcutaneous) white adipose tissue (iWAT) (Fig. 4D-E). By
179 the time the mice reached 40 weeks of age, female KO mice weighed ~ 6 g (20 %) heavier than the WT controls.
180 Increased weight gain over time was not attributed to differences in food intake, as measured manually over a 24 h
181 period (Fig. 4F). Fecal output, frequency, and energy content were also not different between genotypes (Fig. 4G),
182 suggesting that weight gain was not due to greater nutrient absorption. Deep colon temperatures in both light and
183 dark cycle were also not different between genotypes (Fig. 4H). Indirectly calorimetry analyses also revealed no
184 significant differences between genotypes in food intake, physical activity, and energy expenditure across the
185 circadian cycle and metabolic states (*ad libitum* fed, fasted, refed) (Fig. 4I-K). Despite significantly greater body
186 weight and adiposity, female KO mice had the same metabolic profile as the lean WT controls. There were no
187 differences in fasting blood glucose, serum insulin, triglyceride, cholesterol, NEFA, and β -hydroxybutyrate levels
188 between genotypes (Fig. 4L). Interestingly, VLDL-TG levels were lower in female KO mice whereas HDL-
189 cholesterol level was not different between genotypes (Fig. 4M). Direct assessments of glucose handling capacity
190 and insulin sensitivity by glucose and insulin tolerance tests, respectively, also revealed no differences between
191 genotypes (Fig. 4N-O). Together, these data indicate that *Ctrp10*-KO female mice fed LFD develop obesity, but
192 preserve a largely healthy metabolic profile similar to the much leaner WT female mice.

193

194 **Rapid weight gain in CTRP10-deficient female mice fed a high-fat diet**

195 Next, we challenged the mice with a HFD to determine if the sex-dependent effects on body weight become more
196 pronounced. When fed a HFD, body weight gain and body composition were not different between genotypes in

197 male mice (Fig. 5A-B). Food intake, physical activity, and energy expenditure were also not different between
198 genotypes in male mice across the circadian cycle (light and dark) and metabolic states (*ad libitum* fed, fasted,
199 refed) (Fig. 5C-E). In striking contrast, female KO mice gained weight rapidly on HFD (~9 g or 28% heavier) and
200 had greater adiposity than the WT controls (Fig. 5F-H). Surprisingly, food intake, physical activity, and energy
201 expenditure were not significantly different between genotypes in female mice (Fig. 5I-K). The ANCOVA analysis
202 of energy expenditure using body weight as a covariate also did not reveal any differences between genotypes in
203 female mice (Fig. 5L). Interestingly, the respiratory quotient (RER) was significantly lower in female KO mice
204 relative to WT controls, especially during fasting and refeeding (Fig. 5M), suggesting a greater reliance on lipid
205 substrates for energy metabolism during those periods. Together, these data indicate that CTRP10 is required for
206 female-specific body weight control in response to caloric surplus, but neither food intake, physical activity level,
207 nor energy expenditure could account for the marked increase in body weight and adiposity.

208

209 **Obesity is uncoupled from insulin resistance and dyslipidemia in CTRP10-deficient female mice fed a HFD**

210 We again measured fasting and refeeding responses in WT and *Ctrp10*-KO mice fed a HFD. No differences in
211 fasting and refeeding blood glucose, serum insulin, triglyceride, cholesterol, NEFA, and β -hydroxybutyrate levels
212 were noted between genotypes in male mice (Fig. 6A). Female KO mice, however, had higher fasting blood
213 glucose and serum insulin levels, and lower β -hydroxybutyrate levels compared to the WT controls (Fig. 6B). In the
214 refed state, serum insulin levels continued to be significantly higher in female KO mice. Unlike the WT female
215 mice where refeeding markedly lowered serum β -hydroxybutyrate (ketone) levels as expected, KO female mice
216 appeared unable to suppress serum β -hydroxybutyrate levels in response to refeeding (Fig. 6B).

217 Consistent with the fasting blood glucose and insulin data, glucose handling capacity and insulin sensitivity
218 assessments by glucose and insulin tolerance in HFD-fed male mice also revealed no differences between
219 genotypes (Fig. 6C-D). Female KO mice, however, had higher fasting blood glucose and serum insulin levels
220 suggesting the presence of mild insulin resistance (Fig. 6B). We therefore expected to see differences in either
221 glucose and/or insulin tolerance tests. To our surprise, the rate of glucose clearance in response to glucose or insulin
222 injection was virtually identical between WT and KO female mice (Fig. 6E-F), suggesting no difference in insulin
223 sensitivity between genotypes. VLDL-TG and HDL-cholesterol profiles were also indistinguishable between WT
224 and KO female mice (Fig. 6G). Altogether, these data indicate that CTRP10 is not required for metabolic

225 homeostasis in male mice challenged with a HFD. In female mice, however, loss of CTRP10 markedly promotes
226 weight gain in the face of caloric surplus, but, paradoxically, the excess adiposity is largely uncoupled from
227 obesity-linked insulin resistance and dysregulated glucose and lipid metabolism.

228

229 **Obesity is uncoupled from adipose dysfunction and hepatic steatosis in *Ctrp10*-KO female mice fed a HFD**

230 Consistent with greater fat mass in visceral (gonadal) fat depot of *Ctrp10*-KO female mice (Fig. 7A), histological
231 analysis and quantification also indicated significantly larger adipocyte cell size (Fig. 7B). Although the
232 subcutaneous (inguinal) fat pad weight was also significantly heavier in female KO mice (Fig. 7C), the adipocyte
233 cell size was marginally bigger but not significant (Fig. 7D). A bigger fat pad with only marginally larger cell size
234 suggests greater adipocyte hyperplasia in the subcutaneous depot. Increased adipogenesis in response to caloric
235 surfeit is known to be associated with improved systemic metabolic profile (66).

236 Obesity is known to be associated with low-grade inflammation (67), fibrosis (68), and ER and oxidative
237 stress (69, 70). Despite marked differences in body weight and adiposity, the expression of genes associated with
238 inflammation (except for *Ccr2*), fibrosis, oxidative stress in gWAT and iWAT were not significantly different
239 between female KO mice and WT controls (Fig. 7E). The expression of some genes associated with ER stress
240 (e.g., *Ddit3/CHOP*, *Atf4*, *Xbp1*) in iWAT were actually lower in female KO mice (Fig. 7E). Corroborating the gene
241 expression data, quantification of hydroxyproline (marker of fibrosis) and malondialdehyde (marker of oxidative
242 stress) revealed no significant differences between genotypes (Fig. 7F-G).

243 The liver weight of female KO mice was modestly increased (Fig. 7F), but when normalized to body
244 weight it was not significantly different from WT controls (2.76 % in WT and 2.60% in KO, $P = 0.24$). Histological
245 analysis and quantification revealed no differences in hepatic lipid content (% lipid area) between genotypes (Fig.
246 7G). Interestingly, although hepatic fat content was similar between genotypes, the expression of lipogenic genes
247 (e.g., *Fasn*) was lower and fat catabolism genes (e.g., *Cpt2*, *Ppara*, *Acadl*, *Acadm*, *Acad11*, *Acadvl*) was higher in
248 female KO mice (Fig. 7H). The expression of genes associated with inflammation, fibrosis, ER and oxidative stress
249 in liver were not significantly different between genotypes (Fig. 7H). Consistent with the gene expression data,
250 quantification of hydroxyproline (marker of fibrosis) in the liver revealed no significant difference between
251 genotypes (Fig. 7K). The *Ctrp10* KO female mice, however, had higher levels of malondialdehyde (a marker of
252 oxidative stress) in the liver, suggesting a modest increase in oxidative stress (Fig. 7L). Altogether, these data

253 indicate that obesity is largely uncoupled from inflammation, fibrosis, ER and oxidative stress in *Ctrp10* KO female
254 mice.

255

256 **Transcriptomic and pathway changes associated with the metabolically healthy obesity phenotype in *Ctrp10***
257 **KO female mice.**

258 To define the specific mechanisms mediating the female-specific effects of *Ctrp10* ablation on favorable metabolic
259 outcomes, four major metabolic tissues (gWAT, iWAT, liver, skeletal muscle) from female WT and KO mice fed a
260 HFD were subjected to RNA-sequencing. Comparison of differentially expressed genes (DEGs) via limma (71)
261 showed robust changes across tissues, with the largest changes seen in the liver (Fig. 8A-D). In liver, gWAT, and
262 muscle, we observed comparable numbers of DEGs that were up- and down-regulated, whereas more genes were
263 transcriptionally suppressed in the iWAT of *Ctrp10* KO female mice (Fig. 8E, top panel). While significant DEGs
264 were identified in all 4 tissues, only limited overlap was observed between the DEGs in each tissue (Fig. 8E,
265 bottom panel). Gene set enrichment analyses of the DEGs highlighted distinct and shared processes up- or down-
266 regulated across the four tissues (Fig. 8F). Pathways and processes related to lipid metabolism and estrogen
267 receptor were the top-ranked up-regulated enrichments across tissues (Fig. 8F, top panel), whereas processes related
268 to blood clotting and lipoprotein metabolism were the top-ranked down-regulated enrichments (Fig. 8F, bottom
269 panel).

270

271 Of the DEGs, we found significant changes across tissues in relevant classes of genes that encode proteins
272 involved in gene expression (e.g., transcription factors), signaling (e.g., receptors), tissue crosstalk (e.g., secreted
273 proteins), and metabolism (Fig. 9). Notably, the nuclear receptor, *Nr1d1* (also known as *Rev-Erba*), is the only gene
274 consistently suppressed across all four tissues (liver, gWAT, iWAT, and muscle) of *Ctrp10* KO female mice (Fig.
275 8E lower panel and Fig. 9). Interestingly, global deletion of *Nr1d1* promotes lipogenesis, adipose tissue expansion,
276 and obesity (72, 73). Although the whole-body and adipose-specific *Nr1d1* KO mice fed with HFD become
277 markedly obese, the obesity is not accompanied by insulin resistance, adipose tissue inflammation and fibrosis (73,
278 74). Like the *Ctrp10* KO female mice, HFD-fed mice lacking *Nr1d1* can maintain a relatively healthy metabolic
279 profile despite being strikingly obese. Since only male mice were used in these previous studies, we do not know
280 whether female mice lacking *Nr1d1* would also exhibit similar insulin-sensitive obesity phenotype. In WT mice,

281 Nr1d1 acts as a transcriptional repressor of metabolic genes whose expression are upregulated by high-fat feeding;
282 loss of Nr1d1 is thought to result in the de-repression of these genes, leading to greater lipid synthesis and fat mass
283 accrual in response to caloric excess (74). Thus, the suppression of *Nr1d1* expression—mimicking Nr1d1
284 deficiency—across tissues in HFD-fed *Ctrp10* KO female mice may contribute to benign fat mass expansion
285 without the accompanying adipose tissue fibrosis, inflammation, and oxidative stress.

286

287 Among the upregulated genes, *Fgf21* and *Fgf1* was significantly elevated in the liver of *Ctrp10* KO female
288 mice (Fig. 9A). FGF21 is an hepatokine known to improve systemic insulin sensitivity and to promote a favorable
289 metabolic profile in diet-induced obese mice (75). Likewise, FGF1 has been shown to dampen hepatic glucose
290 output by suppressing adipose lipolysis (76), improve systemic insulin sensitivity by reducing adipose
291 inflammation (77), and alleviate hepatic steatosis, inflammation, and insulin resistance (78). Thus, upregulated
292 expression of *Fgf21* and *Fgf1* in *Ctrp10* KO female mice could contribute to the MHO phenotype. In addition, the
293 upregulated hepatic expression of IL-22 receptor (*Il22ra1*) in *Ctrp10* KO female mice (Fig. 9A) may confer
294 protection against obesity-associated fatty liver, inflammation and fibrosis (79-81). Further, a marked increase in
295 uncoupling protein 3 (*Ucp3*) and Krüppel-like factor 15 (*Klf15*) expression in the skeletal muscle (Fig. 9C) may
296 promote lipid utilization and help mitigate lipid-induced insulin resistance in *Ctrp10* KO female mice (82, 83).
297 Taken together, these combined changes—at the level of gene expression and biological pathways and processes
298 across tissues—acting in concert likely contribute to the apparently healthy obesity phenotype seen in the KO
299 female mice.

300

301 **Conservation of mouse DEG co-correlation in humans highlights sex-specific gene connectivity.**

302 Next, we asked whether the female-specific transcriptomic effects across tissues were conserved in humans. To
303 address this, we analyzed transcriptional co-correlation of mouse DEG (Fig. 10) orthologues in GTEx (84),
304 consisting of 210 males and 100 females filtered for comparison of gene expression across tissues (85, 86).
305 Hierarchical clustering of transcriptional correlation of the orthologous DEGs among 4 metabolic tissues—
306 subcutaneous and visceral white adipose tissue, liver, and skeletal muscle—showed differing patterns of gene
307 connectivity between females (Fig. 10A) and males (Fig. 10B). When grouped according to sex in each tissue, the
308 degree of sex-specific gene correlation pairs of DEGs orthologues showed the most significant differences in

309 subcutaneous adipose tissue (Fig. 10C). Given the whole-body metabolic effects of *Ctrp10* ablation in mice, we
310 further examined the degree of sex-dependent DEG co-correlation across metabolic tissues. This analysis showed
311 that human orthologue genes in subcutaneous adipose tissue (Fig. 10D, top row) and liver (Fig. 10D, third row) also
312 exhibited highly significant sex differences in their transcriptional correlation with other DEGs across key
313 metabolic tissues (Fig. 10D). These analyses highlight the sex-specificity of CTRP10 DEG orthologues in humans,
314 suggest possible sex-biased mechanisms of tissue crosstalk, and overall underscores the conservation of the sex-
315 dependent metabolic function of CTRP10.

316

317 **DISCUSSION**

318

319 Our current study has established a novel function for CTRP10 in modulating body weight in a sex-specific
320 manner. When mice were fed a control LFD, female *Ctrp10*-KO mice developed obesity with age; increased
321 adiposity, however, did not impair insulin action and glucose and lipid metabolism. When challenged with an
322 obesogenic diet, female *Ctrp10*-KO mice gained weight rapidly. Despite having strikingly higher adiposity and
323 weighing ~10-11 g (~28%) more, female KO mice fed a HFD exhibited a metabolic profile largely
324 indistinguishable from the much leaner WT controls. Although female KO mice had higher fasting glucose and
325 insulin levels, direct assessments of glucose metabolism and insulin sensitivity by glucose and insulin tolerance
326 tests, however, revealed no differences between genotypes. Except having lower fasting ketone (β -hydroxybutyrate)
327 levels, the fasting lipid profile, as well as VLDL-TG and HDL-cholesterol levels, of *Ctrp10*-KO female mice
328 resembled the WT controls. The hepatic fat content was also comparable between genotypes. Global transcriptomic
329 profiling across different fat depots and liver did not reveal gene expression signatures associated with elevated
330 inflammation, fibrosis, and ER and oxidative stress. Altogether, these findings suggest that CTRP10 deficiency
331 promotes obesity in females but it also uncouples obesity from insulin resistance, dyslipidemia, steatosis,
332 inflammation, and oxidative stress. Thus, *Ctrp10*-KO female mice represent a novel model of female obesity with
333 largely preserved insulin sensitivity and metabolic health.

334

335 Our findings help inform ongoing studies on metabolically healthy obese (MHO) humans (87-92). Because
336 the criteria used to define MHO differs between studies, there is an ongoing debate regarding the prevalence of

337 MHO and what fraction of the MHO population is insulin-sensitive and metabolically healthy (93, 94).
338 Nevertheless, among the obese individuals, there clearly exists a subgroup that maintains long-term normal insulin
339 sensitivity and does not appear to develop any component of the metabolic syndrome (93). MHO is observed in
340 both sexes, but more common in females (6). The underlying mechanism(s) that uncouple obesity from adverse
341 metabolic health in MHO is not well understood (7, 89, 93). It is currently unknown whether males and females
342 with MHO use similar or distinct mechanism to maintain insulin sensitivity and metabolic health. Our findings in
343 *Ctrp10*-KO female, but not male, mice suggest that there may be female-biased mechanism that prevents metabolic
344 deterioration in the face of obesity, thus underscoring the utility of the *Ctrp10*-KO mice as a female mouse model
345 of MHO.

346

347 Obesity is frequently associated with insulin resistance, dyslipidemia, fatty liver, oxidative stress, and
348 chronic low-grade inflammation (67, 95, 96). The mechanisms that link obesity to metabolic dysfunctions are
349 complex and multifactorial. There are limited number of mouse models described where obesity is uncoupled from
350 insulin resistance and metabolic health (97-100); in some studies, however, only male mice were used or that the
351 sex of the animals was not specified. In the case of aP2/FABP4 KO male mice, the uncoupling of obesity from
352 insulin resistance was attributed to a marked decrease in TNF- α expression in adipose tissue (98). In the case of
353 adiponectin overexpression in leptin-deficient (*ob/ob*) male and female mice, a dramatic expansion of the
354 subcutaneous fat pad is thought to promote lipid sequestration in adipose compartment, thus preventing ectopic
355 lipid deposition in non-adipose tissues (e.g., liver, pancreas, muscle) that would otherwise induce insulin resistance
356 (97). Massive obesity with preserved insulin sensitivity is also observed in leptin-deficient (*ob/ob*) male and female
357 mice overexpressing the mitochondrial membrane protein, mitoNEET (100). The benign obesity is attributed to the
358 inhibition of iron transport into mitochondria by mitoNEET, leading to reduced mitochondrial activity, fatty acid
359 oxidation, and oxidative stress (100). In the *Brd2* hypomorphic mice, severe obesity with lower blood glucose and
360 enhanced glucose tolerance is due to a combination of hyperinsulinemia and marked reduction in macrophage
361 infiltration into fat depot (101). Lastly, in male mice fed a high starch diet, uncoupling of obesity from insulin
362 resistance is associated with lower ceramide levels in liver and skeletal muscle (99). In all these cases, the
363 uncoupling of obesity from metabolic dysfunction is seen in either male mice only (female mice were not included)

364 or both sexes. These previous studies suggest that multiple mechanisms, not mutually exclusive, can contribute to
365 the MHO phenotype in different mouse models.

366

367 In our study, loss of CTRP10 in female mice largely uncoupled obesity from insulin resistance,
368 dyslipidemia, steatosis, inflammation, and ER and oxidative stress. The preservation of insulin sensitivity in *Ctrp10*
369 KO female mice is due, at least in part, to the absence of obesity-linked adipose and liver inflammation, fibrosis,
370 and oxidative stress. These phenotypes associated with a favorable metabolic profile are also observed in MHO
371 individuals (88, 102). A healthy adaptive remodeling of white adipose tissues in response to caloric surfeit helps
372 preserve the storage and secretory function of adipocytes (103). The expansion of benign adipose tissues further
373 serves to sequester circulating lipids and prevent their ectopic deposition in non-adipose tissue (e.g., liver and
374 skeletal muscle) which can impair insulin action (104, 105). The MHO phenotype seen in *Ctrp10* KO female mice
375 reinforce the notion that adipose tissue health, rather than abundance, is an important determinant of metabolic
376 health in obesity.

377

378 Because lipidomic analysis was not performed—a limitation of this study—we do not know whether
379 *Ctrp10*-KO female mice have reduced ceramide or diacylglycerol levels in liver and skeletal muscle, two lipid
380 species known to antagonize insulin action (106, 107). However, our global transcriptomic and pathway enrichment
381 analysis across visceral and subcutaneous fat depots, liver, and skeletal muscle highlighted the relevant up- and
382 down-regulated pathways and processes (e.g., lipid and lipoprotein metabolism, signaling) that may contribute to
383 the MHO phenotype in *Ctrp10*-KO female mice. How these changes across tissues help to suppress the deleterious
384 effects of obesity and maintain an apparently healthy metabolic profile in *Ctrp10*-KO female mice remains to be
385 fully understood. Part of the mechanism may be attributable to the suppression of *Nr1d1* and the upregulated
386 expression of *Fgf1*, *Fgf21*, *Il22ra1*, *Ucp3*, *Klf15*. Altered expression of these genes are known to reduce obesity-
387 linked inflammation, oxidative stress, steatosis, and insulin resistance.

388

389 In many single-gene KO mouse models where both sexes are examined, it is often the males that show a
390 more pronounced metabolic phenotype. It is known that C57BL/6 female mice generally gain significantly less
391 weight on HFD compared to male mice (108). Therefore, it is intriguing that *Ctrp10*-KO female mice became obese

392 on a control LFD and gained weight rapidly when fed an obesogenic diet. After twelve weeks on HFD, the body
393 weight of female KO mice was approaching that of WT male mice fed the same diet. What mechanism underlies
394 the sexually dimorphic requirement of CTRP10 for body weight control? We know that the obesity phenotype was
395 not attributed to differences in food intake, physical activity level, body temperature, and energy expenditure
396 between WT and KO female mice. We assume that the methods used to quantify these physiologic parameters are
397 sensitive enough to detect small differences that can give rise to divergent body weight over time. Quantification of
398 fecal output and fecal energy content also revealed no differences between genotypes. Thus, loss of CTRP10 did
399 not affect macronutrient intake and absorption. Although we cannot fully rule out the CNS function of
400 CTRP10/C1QL2 (62), our data do not support a central role for CTRP10 in modulating food intake behavior,
401 locomotor activity, and energy expenditure that affect body weight in female mice.

402

403 It is known that reduced estrogen level by ovariectomy or blocking estrogen action in estrogen receptor
404 ($ER\alpha$) KO mice will cause obesity and metabolic dysfunction in female mice fed a HFD (109-111). Conversely,
405 estradiol supplementation decreases HFD-induced weight gain and improves glucose tolerance and insulin
406 sensitivity (112-114). Estrogen also has the effect of reducing food intake, and promoting physical activity and
407 energy expenditure (115-119). In our study, loss of CTRP10 promotes obesity without altering food intake,
408 physical activity, and energy expenditure. While estrogen's role cannot be completely ruled out, the fact that female
409 *Ctrp10*-KO mice developed obesity with largely preserved metabolic health suggest that factors other than altered
410 estrogen level contribute to the insulin-sensitive obesity phenotype. Future studies are warranted to uncover what
411 factor(s) is causally contributing to obesity in female mice lacking CTRP10.

412

413 The sex-dependent effects of CTRP10 on metabolism and tissue transcriptomes appear to be conserved in
414 humans. When the human orthologues of the mouse DEGs were used to interrogate the GTEx data, clear patterns of
415 gene connectivity within and across metabolic tissues in females and males were observed, with the strongest sex-
416 specific gene correlations seen in subcutaneous adipose tissue and liver. These findings provide further evidence
417 that CTRP10 modulates tissue transcriptome in a sex-dependent manner. Further, our analyses of sex-dependent
418 DEG co-correlation across metabolic tissues also suggest possible sex-biased mechanisms of inter-organ metabolic
419 signaling between adipose tissue and liver.

420

421 CTRP10 has been previously shown to bind to the adhesion GPCR, brain angiogenesis inhibitor-3
422 (Bai3/Adgrb3) (120). Bai3 is expressed in the brain and peripheral tissues, and it is a promiscuous GPCR that can
423 bind to multiple ligands. In addition to CTRP10 (C1QL2), Bai3 also binds to CTRP11 (C1QL4), CTRP13
424 (C1QL3), CTRP14 (C1QL1), neuronal pentraxins, and reticulon 4 (RTN4) receptor (56, 58, 59, 120-122). A
425 constitutive, whole-body KO of Bai3 mouse models have recently been generated (123, 124). Both male and female
426 *Bai3* KO mice fed a standard chow have significantly lower body weight, beginning at weaning (3 weeks old) and
427 continue into adulthood (123, 124). Lower body weight in *Bai3* KO mice of either sex is attributed to a reduction in
428 both lean and fat mass, and is associated with higher energy expenditure and reduced food intake in male mice
429 (123). The impact of Bai3 deficiency on systemic metabolism in response to a high-fat diet was not examined. The
430 *Ctrp10* KO mice do not phenocopy the phenotypes of the *Bai3* KO mice. When fed a control low-fat diet, the body
431 weight, food intake, and energy expenditure of *Ctrp10* KO male mice were indistinguishable from WT controls. In
432 striking contrast to *Bai3* KO mice, female *Ctrp10* KO mice fed a low-fat diet began to gain more weight around 20
433 weeks of age, and by 40 weeks had become visibly obese. While we did not rule out CTRP10-Bai3 signaling axis
434 in modulating energy metabolism in peripheral tissues, our findings in *Ctrp10* KO mice suggest that future works
435 are needed to establish the molecular mechanisms that mediate the systemic metabolic function of CTRP10.

436

437 Several limitations of our current study are noted. We use a constitutive whole-body KO mouse model of
438 CTRP10 to interrogate its function. It is unknown whether CTRP10 has a role during development that may
439 influence sex-dependent postnatal weight gain with age or in response to a high-caloric diet. Future studies using
440 conditional KO of *Ctrp10* gene in adult mice can help address this issue. Although the lack of differences in food
441 intake, physical activity, and energy expenditure between genotypes do not support a central role of CTRP10 in
442 mediating the metabolic phenotypes of *Ctrp10*-KO female mice, a brain-specific KO of *Ctrp10* gene is needed to
443 definitively rule this out. Our phenotypic analyses in the context of metabolism are relatively comprehensive but
444 not exhaustive. Although the metabolic profile of obese *Ctrp10*-KO female mice was largely indistinguishable from
445 the much leaner WT controls, we do not know if some related aspect of metabolic health (e.g., blood pressure and
446 heart function) may be altered in the absence of CTRP10 which we did not examine.

447

448 In summary, we have established the physiologic role and requirement of CTRP10 in modulating body
449 weight in a female-specific manner. Importantly, loss of CTRP10 largely uncouples obesity from insulin resistance
450 and metabolic dysfunction. The CTRP10-deficient female mice represent a unique and valuable model to help
451 dissect female-biased mechanisms that help preserve metabolic health in the face of positive energy balance and
452 increased adiposity.

453

454 **MATERIALS AND METHODS**

455

456 **Mouse models**

457 Eight-week-old mouse tissues (gonadal and inguinal white adipose tissues, interscapular brown adipose tissue,
458 liver, heart, skeletal muscle, kidney, pancreas, cerebellum, cortex, hippocampus, hindbrain, and hypothalamus)
459 from C57BL/6J male mice (The Jackson Laboratory, Bar Harbor, ME) were collected from fasted and refed
460 experiments as we have previously described (125). For the fasted group, food was removed for 16 h (beginning 10
461 h into the light cycle), and mice were euthanized 2 h into the light cycle. For the refed group, mice were fasted for
462 16 h and refed with chow pellets for 2 h before being euthanized. Tissues (white and brown adipose tissues, liver,
463 whole brain, kidney, spleen, heart, skeletal muscle, pancreas, small intestine, and colon) from C57BL/6J male mice
464 fed a low-fat diet (LFD) or a high-fat diet (HFD) for 12 weeks were also collected as we have previously described
465 (125).

466 The *Ctrp10/C1ql2*-KO mice (C57BL/6N^{CrI}-*C1ql2*^{em1(IMPC)Mbp}/Mmucd; stock number 050587-UCD) were
467 generated using the CRISPR-cas9 method at UC Davis. The two guide RNAs (gRNA) used were 5'-CCGGCGCC
468 GCTCCACCATTACCT-3' and 5'-TCAGGCCACCCCATCCCCATCGG-3'. The *Ctrp10* gene consists of 2 exons.
469 The entire protein coding region spanning exon 1 and 2 was deleted. This KO strategy ensures a complete null
470 allele for *Ctrp10*. The KO mice were maintained on a C57BL6/6J genetic background. Genotyping primers for WT
471 allele were forward (m10-Com-F) 5'-TGTCGGGCTCTTCGACTCTCCA-3' and reverse (m10-WT-R) 5'-
472 GCATCTCGT AGTGAGCCGCTCC-3'. The size of the WT band was 360 bp. Genotyping primers for the *Ctrp10*
473 KO allele were forward (m10-Com-F) 5'-TGTCGGGCTCTTCGACTCTCCA-3' and reverse (m10-Mut-R1) 5'-
474 GTCCAATCAGCT TTCTCAAGTCTGG-3'. The size of the KO band was 422 bp. The genotyping PCR
475 parameters were as follows: 94°C for 5 min, followed by 10 cycles of (94°C for 10 sec, 65°C for 15 sec, 72°C for

476 30 sec), then 25 cycles of (94°C for 10 sec, 55°C for 15 sec, 72°C for 30 sec), and lastly 72°C for 5 min. Due to the
477 presence of GC rich sequences, 7% DMSO was included in the PCR genotyping reaction. Mice were generated by
478 intercrossing *Ctrp10* heterozygous (+/-) mice, supplemented with intercrossing WT or KO mice. *Ctrp10* KO (-/-)
479 and WT (+/+) controls were housed in polycarbonate cages on a 12-h light–dark photocycle with ad libitum access
480 to water and food. Mice were fed either a control low-fat diet (LFD; 10% kcal derived from fat; # D12450B;
481 Research Diets, New Brunswick, NJ) or a high-fat diet (HFD; 60% kcal derived from fat; #D12492, Research
482 Diets). LFD was provided for the duration of the study, beginning at 5 weeks of age; HFD was provided for 14
483 weeks, beginning at 6-7 weeks of age. At termination of study, all mice were fasted for 2 h and euthanized. Tissues
484 were collected, snap-frozen in liquid nitrogen, and kept at -80°C until analysis. All mouse protocols (protocol #
485 MO22M367) were approved by the Institutional Animal Care and Use Committee of the Johns Hopkins University
486 School of Medicine. All animal experiments were conducted in accordance with the National Institute of Health
487 guidelines and followed the standards established by the Animal Welfare Acts.

488

489 **Body composition analysis**

490 Body composition analyses for total fat, lean mass, and water content were determined using a quantitative
491 magnetic resonance instrument (Echo-MRI-100, Echo Medical Systems, Waco, TX) at the Mouse Phenotyping
492 Core facility at Johns Hopkins University School of Medicine.

493

494 **Indirect calorimetry**

495 LFD- or HFD-fed WT and *Ctrp10* KO male and female mice were used for simultaneous assessments of daily body
496 weight change, food intake (corrected for spillage), physical activity, and whole-body metabolic profile in an open
497 flow indirect calorimeter (Comprehensive Laboratory Animal Monitoring System, CLAMS; Columbus
498 Instruments, Columbus, OH) as previously described (25). In brief, data were collected for three days to confirm
499 mice were acclimatized to the calorimetry chambers (indicated by stable body weights, food intakes, and diurnal
500 metabolic patterns), and data were analyzed from the fourth day. Rates of oxygen consumption (\dot{V}_{O_2} ; mL·kg⁻¹·h⁻¹)
501 and carbon dioxide production (\dot{V}_{CO_2} ; mL·kg⁻¹·h⁻¹) in each chamber were measured every 24 min throughout the
502 studies. Respiratory exchange ratio (RER = $\dot{V}_{CO_2}/\dot{V}_{O_2}$) was calculated by CLAMS software (version 5.66) to
503 estimate relative oxidation of carbohydrates (RER = 1.0) versus fats (RER = 0.7), not accounting for protein

504 oxidation. Energy expenditure (EE) was calculated as $EE = \dot{V}_{O_2} \times [3.815 + (1.232 \times RER)]$ and normalized to lean
505 mass. Because normalizing to lean mass can potentially lead to overestimation of EE, we also performed ANCOVA
506 analysis on EE using body weight as a covariate (126). Physical activities were measured by infrared beam breaks
507 in the metabolic chamber.

508 **Measurements of 24 h food intake**

509 To independently confirm the food intake data collected in the metabolic cage (CLAMS), we also performed 24 h
510 food intake measurements manually. All mice were singly housed, with wire mesh flooring inserts over a piece of
511 cage paper on the bottom of the cage. A known weight of food pellets was given to each mouse. Twenty-four hours
512 later, the leftover food pellets remaining on the flooring insert, along with any spilled crumbs on the cage paper,
513 were collected and weighed. Thus, food intake was corrected for spillage.

514

515 **Glucose, insulin, pyruvate, and lipid tolerance tests**

516 All tolerance tests were conducted as previously described (21, 24, 29). For glucose tolerance tests (GTTs), mice
517 were fasted for 6 h before glucose injection. Glucose (Sigma, St. Louis, MO) was reconstituted in saline (0.9 g
518 NaCl/L), sterile-filtered, and injected intraperitoneally (i.p.) at 1 mg/g body weight (i.e., 10 μ L/g body weight).
519 Blood glucose was measured at 0, 15, 30, 60, and 120 min after glucose injection using a glucometer (NovaMax
520 Plus, Billerica, MA). For insulin tolerance tests (ITTs), food was removed 2 h before insulin injection. 6.5 μ L of
521 insulin stock (4 mg/mL; Gibco) was diluted in 10 mL of saline, sterile-filtered, and injected i.p. at 0.75 U/kg body
522 weight (i.e., 10 μ L/g body weight). Blood glucose was measured at 0, 15, 30, 60, and 90 min after insulin injection
523 using a glucometer (NovaMax Plus).

524

525 **Fasting-Refeeding insulin tests**

526 Mice were fasted overnight (~16 h) then reintroduced to food as described (26). Blood glucose was monitored at
527 the 16 h fast time point (time = 0 h refed) and at 1 and 2 hours into the refeeding process. Serum was collected at
528 the 16 h fast and 2 h refed time points for insulin ELISA, as well as for the quantification of triglyceride,
529 cholesterol, non-esterified free fatty acids (NEFA), and β -hydroxybutyrate levels.

530

531 **Blood and tissue chemistry analysis**

532 Tail vein blood samples were allowed to clot on ice and then centrifuged for 10 min at 10,000 x g. Serum samples
533 were stored at -80°C until analyzed. Serum triglycerides (TG) and cholesterol levels were measured according to
534 manufacturer's instructions using an Infinity kit (Thermo Fisher Scientific, Middletown, VA). Non-esterified free
535 fatty acids (NEFA) were measured using a Wako kit (Wako Chemicals, Richmond, VA). Serum β -hydroxybutyrate
536 (ketone) concentrations were measured with a StanBio Liquicolor kit (StanBio Laboratory, Boerne, TX). Serum
537 insulin levels were measured by ELISA according to manufacturer's instructions (Crystal Chem, Elk Grove
538 Village, IL; cat # 90080). Hydroxyproline assay (Sigma Aldrich, MAK008) was used to quantify total collagen
539 content in liver and adipose tissues according to the manufacturer's instructions. Lipid peroxidation levels (marker
540 of oxidative stress) in the liver and adipose tissues were assessed by the quantification of malondialdehyde (MDA)
541 via Thiobarbituric Acid Reactive Substances (TBARS) assay (Cayman Chemical, 700870) according to the
542 manufacturer's instructions.

543 544 **Serum lipoprotein triglyceride and cholesterol analysis by FPLC**

545 Food was removed for 2-4 hr (in the light cycle) prior to blood collection. Sera collected from mice were pooled (n
546 = 6-7/genotype) and sent to the Mouse Metabolism Core at Baylor College of Medicine for analysis. Serum
547 samples were first fractionated by fast protein liquid chromatography (FPLC). A total of 45 fractions were
548 collected, and TG and cholesterol in each fraction was quantified.

549 550 **Histology and quantification**

551 Inguinal (subcutaneous) white adipose tissue (iWAT), gonadal (visceral) white adipose tissue (gWAT), and liver
552 were dissected and fixed in formalin. Paraffin embedding, tissue sectioning, and staining with hematoxylin and
553 eosin were performed at the Pathology Core facility at Johns Hopkins University School of Medicine. Images were
554 captured with a Keyence BZ-X700 All-in-One fluorescence microscope (Keyence Corp., Itasca, IL). Adipocyte
555 (gWAT and iWAT) cross-sectional area (CSA), as well as the total area covered by lipid droplets in hepatocytes
556 were measured on hematoxylin and eosin-stained slides using ImageJ software (127). For CSA measurements, all
557 cells in one field of view at 100X magnification per tissue section per mouse were analyzed. Image capturing and
558 quantifications were carried out blinded to genotype.

559

560 **Fecal bomb calorimetry and assessment of fecal parameters**

561 Fecal pellet frequency and average fecal pellet weight were monitored by housing each mouse singly in clean cages
562 with a wire mesh sitting on top of a cutout cardboard that lay at the bottom of the cage for fecal collection. The
563 number of fecal pellets and their total weight was recorded at the end of 24 h period. Additional fecal pellets
564 collected for 3 full days were combined and shipped to the University of Michigan Animal Phenotyping Core for
565 fecal bomb calorimetry. Briefly, fecal samples were dried overnight at 50°C prior to weighing and grinding them to
566 powder. Each sample was mixed with wheat flour (90% wheat flour, 10% sample) and formed into 1.0 g pellet,
567 which was then secured into the firing platform and surrounded by 100% oxygen. The bomb was lowered into a
568 water reservoir and ignited to release heat into the surrounding water. These data were used to calculate fecal pellet
569 frequency (bowel movements/day), average fecal pellet weight (g/bowel movement), fecal energy (cal/g feces), and
570 total fecal energy (kcal/day).

571

572 **Tissue library preparation and RNA sequencing**

573 Total RNA was isolated from tissues using Trizol reagent (Thermo Fisher Scientific) according to the
574 manufacturer's instructions. Library preparation and bulk RNA sequencing of liver, skeletal muscle
575 (gastrocnemius), gonadal white adipose tissue (gWAT), and inguinal white adipose tissue (iWAT) of HFD-fed
576 *Ctrp10*-KO female mice and WT controls were performed by Novogene (Sacramento, California, USA) on an
577 Illumina platform (NovaSeq 6000) and pair-end reads were generated. Sample size: 6 WT and 6 KO for each tissue.
578 All raw sequencing files are available from the NIH Sequence Read Archive (SRA) accession PRJNA971939.

579

580 **Mouse RNA-Sequencing analysis.**

581 Transcript features were assembled from raw fastq files and aligned to the current version of mouse transcriptome
582 (*Mus_musculus.GRCm39.cdna*) using kallisto -aln (128). Version-specific Ensembl transcript IDs were linked to
583 gene symbols using biomaRt. Estimated counts were log normalized and filtered for a limit of sum >5 across all
584 samples. Logistic regressions comparing WT vs KO samples across tissues were performed using limma (71).
585 Differential expression results were visualized using available R packages in CRAN: ggplot2, ggVennDiagram and
586 pheatmap. Gene set enrichment analyses of the DEGs were performed using Enrichr (129). Scripts for analyses and

587 visualization are available at [https://github.com/Leandromvelez/CTRP10-Manuscript-DEG-Sex-specific-](https://github.com/Leandromvelez/CTRP10-Manuscript-DEG-Sex-specific-connectivities-and-integration/)
588 [connectivities-and-integration/](https://github.com/Leandromvelez/CTRP10-Manuscript-DEG-Sex-specific-connectivities-and-integration/)

589

590 **Human sex difference analysis.**

591 All the datasets and scripts to perform analyses are available at: [https://github.com/Leandromvelez/CTRP10-](https://github.com/Leandromvelez/CTRP10-Manuscript-DEG-Sex-specific-connectivities-and-integration/)
592 [Manuscript-DEG-Sex-specific-connectivities-and-integration/](https://github.com/Leandromvelez/CTRP10-Manuscript-DEG-Sex-specific-connectivities-and-integration/). Male and Female human data were obtained from
593 Genotype-Tissue Expression (GTEx) (84) and filtered for sufficient comparison of inter-tissue transcript correlation
594 as described (85, 86). CTRP10/C1QL2 and other human orthologues for mouse differentially expressed genes
595 (DEGs) were identified by intersecting mouse gene symbols with known human orthologues from the vertebrate
596 homology resource at Mouse Genome Informatics (MGI) (130). Co-correlation between all human orthologues
597 DEGs were calculated in either self-reported male or female subjects in GTEx using the `bicorAndPvalue()` function
598 in Weighted Genetic Coexpression Network Analysis (WGCNA) package (131). To compare sex-differences of
599 regression coefficients, wilcoxon t-tests were compared between coefficients using the R package `ggpubr`.

600

601 **Quantitative real-time PCR**

602 Total RNA was isolated from tissues using Trizol reagent (Thermo Fisher Scientific). Purified RNA was reverse
603 transcribed using an iScript cDNA Synthesis Kit (Bio-rad). Real-time quantitative PCR analysis was performed on
604 a CFX Connect Real-Time System (Bio-rad) using iTaqTM Universal SYBR Green Supermix (Bio-rad) according to
605 manufacturer's instructions. Data were normalized to the stable housekeeping gene *β-actin* or *36B4* (encoding the
606 acidic ribosomal phosphoprotein P0) and expressed as relative mRNA levels using the $\Delta\Delta C_t$ method (132). Real-
607 time qPCR primers used to assess *Ctrp10* expression across mouse tissues were: *Ctrp10* forward, 5'-
608 CGGCTTCATGAC ACTTCCTGA-3' and reverse, 5'-AGCAGGGATGTGTCTTTTCCA-3'. qPCR primers used
609 to confirm the absence of *Ctrp10* in KO mice were: forward (qPCR-m10-F2), 5'-
610 CACGTACCACATTCTCATGCG-3' and reverse (qPCR-m10-R1), 5'-TCGTAATTCTGGTCCGCGTC-3'.

611

612 **Statistical analyses**

613 Sample size is indicated in figure and/or figure legend. All results are expressed as mean \pm standard error of the
614 mean (SEM). Statistical analysis was performed with Prism 9 software (GraphPad Software, San Diego, CA). Data

615 were analyzed with two-tailed Student's *t*-tests, one-way ANOVA or two-way ANOVA (with Sidak's post hoc
616 tests). 2-way ANOVA was used for body weight over time, fasting-refeeding response, and all tolerance tests. $P <$
617 0.05 was considered statistically significant.

618

619 **ACKNOWLEDGEMENTS**

620 This work was supported by the National Institutes of Health (DK084171 to GWW, HL138193 and DK130640 to
621 MMS). D.C.S. is supported by an NIH T32 training grant (HL007534). The fecal bomb calorimetry analysis was
622 performed at the University of Michigan Animal Phenotyping Core, supported by center grants 1U2CDK135066-
623 01 (Mi-MPMOD) and DK020572 (MDRC). The FPLC/serum analyses were performed the Mouse Metabolism and
624 Phenotyping Core (MMPC) at the Baylor College of Medicine, supported by NIH grants (DK114356 and
625 UM1HG006348).

626

627 **AUTHOR CONTRIBUTIONS**

628 FC, GWW contributed to the experimental design; FC, DCS, MS, SA, and GWW performed the experiments; FC,
629 DCS, SA, LMV, MMS, and GWW analyzed and interpreted the data; GWW drafted the paper with inputs and edits
630 from all authors.

631

632 **COMPETING INTERESTS**

633 We declare that none of the authors has a conflict of interest.

634

635 **DATA AVAILABILITY**

636 High-throughput sequencing data from this study have been submitted to the NCBI Sequence Read Archive under
637 accession number PRJNA971939. All processed datasets used and R scripts to reproduce analyses are freely
638 available at: [https://github.com/Leandromvelez/CTRP10-Manuscript-DEG-Sex-specific-connectivities-and-
639 integration/](https://github.com/Leandromvelez/CTRP10-Manuscript-DEG-Sex-specific-connectivities-and-integration/).

640

641

642

643

644

645

646

647 REFERENCES

- 648 1. Collaboration, N. C. D. R. F. (2017) Worldwide trends in body-mass index, underweight, overweight, and
649 obesity from 1975 to 2016: a pooled analysis of 2416 population-based measurement studies in 128.9 million
650 children, adolescents, and adults. *Lancet* **390**, 2627-2642
- 651 2. Flier, J. S. (2023) Moderating "the great debate": The carbohydrate-insulin vs. the energy balance models of
652 obesity. *Cell Metab* **35**, 737-741
- 653 3. Bluher, M. (2019) Obesity: global epidemiology and pathogenesis. *Nat Rev Endocrinol* **15**, 288-298
- 654 4. Bouchard, C. (2021) Genetics of Obesity: What We Have Learned Over Decades of Research. *Obesity (Silver*
655 *Spring)* **29**, 802-820
- 656 5. Loos, R. J. F., and Kilpelainen, T. O. (2018) Genes that make you fat, but keep you healthy. *J Intern Med*
657 **284**, 450-463
- 658 6. van Vliet-Ostaptchouk, J. V., Nuotio, M. L., Slagter, S. N., Doiron, D., Fischer, K., Foco, L., Gaye, A.,
659 Gogele, M., Heier, M., Hiekkalinna, T., Joensuu, A., Newby, C., Pang, C., Partinen, E., Reischl, E.,
660 Schwienbacher, C., Tammesoo, M. L., Swertz, M. A., Burton, P., Ferretti, V., Fortier, I., Giepmans, L.,
661 Harris, J. R., Hillege, H. L., Holmen, J., Jula, A., Kootstra-Ros, J. E., Kvaloy, K., Holmen, T. L., Mannisto,
662 S., Metspalu, A., Midthjell, K., Murtagh, M. J., Peters, A., Pramstaller, P. P., Saaristo, T., Salomaa, V., Stolk,
663 R. P., Uusitupa, M., van der Harst, P., van der Klauw, M. M., Waldenberger, M., Perola, M., and
664 Wolffenbuttel, B. H. (2014) The prevalence of metabolic syndrome and metabolically healthy obesity in
665 Europe: a collaborative analysis of ten large cohort studies. *BMC Endocr Disord* **14**, 9
- 666 7. Bluher, M. (2020) Metabolically Healthy Obesity. *Endocr Rev* **41**
- 667 8. Priest, C., and Tontonoz, P. (2019) Inter-organ cross-talk in metabolic syndrome. *Nat Metab* **1**, 1177-1188
- 668 9. Seldin, M. M., Tan, S. Y., and Wong, G. W. (2014) Metabolic function of the CTRP family of hormones. *Rev*
669 *Endocr Metab Disord* **15**, 111-123
- 670 10. Wong, G. W., Wang, J., Hug, C., Tsao, T. S., and Lodish, H. F. (2004) A family of Acrp30/adiponectin
671 structural and functional paralogs. *Proc Natl Acad Sci U S A* **101**, 10302-10307
- 672 11. Seldin, M. M., Peterson, J. M., Byerly, M. S., Wei, Z., and Wong, G. W. (2012) Myonectin (CTRP15), a
673 novel myokine that links skeletal muscle to systemic lipid homeostasis. *J Biol Chem* **287**, 11968-11980
- 674 12. Wei, Z., Peterson, J. M., Lei, X., Cebotaru, L., Wolfgang, M. J., Baldeviano, G. C., and Wong, G. W. (2012)
675 C1q/TNF-related protein-12 (CTRP12), a novel adipokine that improves insulin sensitivity and glycemic
676 control in mouse models of obesity and diabetes. *J Biol Chem* **287**, 10301-10315
- 677 13. Wei, Z., Peterson, J. M., and Wong, G. W. (2011) Metabolic regulation by C1q/TNF-related protein-13
678 (CTRP13): activation of AMP-activated protein kinase and suppression of fatty acid-induced JNK signaling.
679 *J Biol Chem* **286**, 15652-15665
- 680 14. Wei, Z., Seldin, M. M., Natarajan, N., Djemal, D. C., Peterson, J. M., and Wong, G. W. (2013) C1q/Tumor
681 Necrosis Factor-related Protein 11 (CTRP11), a Novel Adipose Stroma-derived Regulator of Adipogenesis. *J*
682 *Biol Chem* **288**, 10214-10229
- 683 15. Wong, G. W., Krawczyk, S. A., Kitidis-Mitrokostas, C., Ge, G., Spooner, E., Hug, C., Gimeno, R., and
684 Lodish, H. F. (2009) Identification and characterization of CTRP9, a novel secreted glycoprotein, from
685 adipose tissue that reduces serum glucose in mice and forms heterotrimers with adiponectin. *FASEB J* **23**,
686 241-258
- 687 16. Wong, G. W., Krawczyk, S. A., Kitidis-Mitrokostas, C., Revett, T., Gimeno, R., and Lodish, H. F. (2008)
688 Molecular, biochemical and functional characterizations of C1q/TNF family members: adipose-tissue-
689 selective expression patterns, regulation by PPAR-gamma agonist, cysteine-mediated oligomerizations,
690 combinatorial associations and metabolic functions. *Biochem J* **416**, 161-177

- 691 17. Ghai, R., Waters, P., Roumenina, L. T., Gadjeva, M., Kojouharova, M. S., Reid, K. B., Sim, R. B., and
692 Kishore, U. (2007) C1q and its growing family. *Immunobiology* **212**, 253-266
- 693 18. Ressler, S., Vu, B. K., Vivona, S., Martinelli, D. C., Sudhof, T. C., and Brunger, A. T. (2015) Structures of
694 C1q-like proteins reveal unique features among the C1q/TNF superfamily. *Structure* **23**, 688-699
- 695 19. Lei, X., Rodriguez, S., Petersen, P. S., Seldin, M. M., Bowman, C. E., Wolfgang, M. J., and Wong, G. W.
696 (2016) Loss of CTRP5 improves insulin action and hepatic steatosis. *Am J Physiol Endocrinol Metab* **310**,
697 E1036-1052
- 698 20. Lei, X., Seldin, M. M., Little, H. C., Choy, N., Klonisch, T., and Wong, G. W. (2017) C1q/TNF-related
699 protein 6 (CTRP6) links obesity to adipose tissue inflammation and insulin resistance. *J Biol Chem* **292**,
700 14836-14850
- 701 21. Lei, X., and Wong, G. W. (2019) C1q/TNF-related protein 2 (CTRP2) deletion promotes adipose tissue
702 lipolysis and hepatic triglyceride secretion. *J Biol Chem* **294**, 15638-15649
- 703 22. Little, H. C., Rodriguez, S., Lei, X., Tan, S. Y., Stewart, A. N., Sahagun, A., Sarver, D. C., and Wong, G. W.
704 (2019) Myonectin deletion promotes adipose fat storage and reduces liver steatosis. *FASEB J* **33**, 8666-8687
- 705 23. Petersen, P. S., Lei, X., Wolf, R. M., Rodriguez, S., Tan, S. Y., Little, H. C., Schweitzer, M. A., Magnuson,
706 T. H., Steele, K. E., and Wong, G. W. (2017) CTRP7 deletion attenuates obesity-linked glucose intolerance,
707 adipose tissue inflammation, and hepatic stress. *Am J Physiol Endocrinol Metab* **312**, E309-E325
- 708 24. Rodriguez, S., Lei, X., Petersen, P. S., Tan, S. Y., Little, H. C., and Wong, G. W. (2016) Loss of CTRP1
709 disrupts glucose and lipid homeostasis. *Am J Physiol Endocrinol Metab* **311**, E678-E697
- 710 25. Sarver, D. C., Stewart, A. N., Rodriguez, S., Little, H. C., Aja, S., and Wong, G. W. (2020) Loss of CTRP4
711 alters adiposity and food intake behaviors in obese mice. *Am J Physiol Endocrinol Metab* **319**, E1084-E1100
- 712 26. Sarver, D. C., Xu, C., Aja, S., and Wong, G. W. (2022) CTRP14 inactivation alters physical activity and food
713 intake response to fasting and refeeding. *Am J Physiol Endocrinol Metab* **322**, E480-E493
- 714 27. Sarver, D. C., Xu, C., Carreno, D., Arking, A., Terrillion, C. E., Aja, S., and Wong, G. W. (2022) CTRP11
715 contributes modestly to systemic metabolism and energy balance. *FASEB J* **36**, e22347
- 716 28. Tan, S. Y., Lei, X., Little, H. C., Rodriguez, S., Sarver, D. C., Cao, X., and Wong, G. W. (2020) CTRP12
717 ablation differentially affects energy expenditure, body weight, and insulin sensitivity in male and female
718 mice. *Am J Physiol Endocrinol Metab* **319**, E146-E162
- 719 29. Tan, S. Y., Little, H. C., Lei, X., Li, S., Rodriguez, S., and Wong, G. W. (2016) Partial deficiency of CTRP12
720 alters hepatic lipid metabolism. *Physiol Genomics* **48**, 936-949
- 721 30. Wei, Z., Lei, X., Petersen, P. S., Aja, S., and Wong, G. W. (2014) Targeted deletion of C1q/TNF-related
722 protein 9 increases food intake, decreases insulin sensitivity, and promotes hepatic steatosis in mice. *Am J*
723 *Physiol Endocrinol Metab* **306**, E779-790
- 724 31. Wolf, R. M., Lei, X., Yang, Z. C., Nyandjo, M., Tan, S. Y., and Wong, G. W. (2016) CTRP3 deficiency
725 reduces liver size and alters IL-6 and TGFbeta levels in obese mice. *Am J Physiol Endocrinol Metab* **310**,
726 E332-345
- 727 32. Peterson, J. M., Seldin, M. M., Tan, S. Y., and Wong, G. W. (2014) CTRP2 overexpression improves insulin
728 and lipid tolerance in diet-induced obese mice. *PLoS One* **9**, e88535
- 729 33. Peterson, J. M., Seldin, M. M., Wei, Z., Aja, S., and Wong, G. W. (2013) CTRP3 attenuates diet-induced
730 hepatic steatosis by regulating triglyceride metabolism. *Am J Physiol Gastrointest Liver Physiol* **305**, G214-
731 224.
- 732 34. Peterson, J. M., Wei, Z., Seldin, M. M., Byerly, M. S., Aja, S., and Wong, G. W. (2013) CTRP9 transgenic
733 mice are protected from diet-induced obesity and metabolic dysfunction. *Am J Physiol Regul Integr Comp*
734 *Physiol* **305**, R522-533
- 735 35. Appari, M., Breitbart, A., Brandes, F., Szaroszyk, M., Froese, N., Korf-Klingebiel, M., Mohammadi, M. M.,
736 Grund, A., Scharf, G. M., Wang, H., Zwadlo, C., Fraccarollo, D., Schrameck, U., Nemer, M., Wong, G. W.,
737 Katus, H. A., Wollert, K. C., Muller, O. J., Bauersachs, J., and Heineke, J. (2017) C1q-TNF-Related Protein-
738 9 Promotes Cardiac Hypertrophy and Failure. *Circ Res* **120**, 66-77
- 739 36. Zheng, Q., Yuan, Y., Yi, W., Lau, W. B., Wang, Y., Wang, X., Sun, Y., Lopez, B. L., Christopher, T. A.,
740 Peterson, J. M., Wong, G. W., Yu, S., Yi, D., and Ma, X. L. (2011) C1q/TNF-Related Proteins, A Family of
741 Novel Adipokines, Induce Vascular Relaxation Through the Adiponectin Receptor-1/AMPK/eNOS/Nitric
742 Oxide Signaling Pathway. *Arterioscler Thromb Vasc Biol* **31**, 2616-2623
- 743 37. Kambara, T., Ohashi, K., Shibata, R., Ogura, Y., Maruyama, S., Enomoto, T., Uemura, Y., Shimizu, Y.,
744 Yuasa, D., Matsuo, K., Miyabe, M., Kataoka, Y., Murohara, T., and Ouchi, N. (2012) CTRP9 protein

- 745 protects against myocardial injury following ischemia-reperfusion through AMP-activated protein kinase
746 (AMPK)-dependent mechanism. *J Biol Chem* **287**, 18965-18973
- 747 38. Kambara, T., Shibata, R., Ohashi, K., Matsuo, K., Hiramatsu-Ito, M., Enomoto, T., Yuasa, D., Ito, M.,
748 Hayakawa, S., Ogawa, H., Aprahamian, T., Walsh, K., Murohara, T., and Ouchi, N. (2015) C1q/Tumor
749 Necrosis Factor-Related Protein 9 Protects against Acute Myocardial Injury through an Adiponectin Receptor
750 I-AMPK-Dependent Mechanism. *Mol Cell Biol* **35**, 2173-2185
- 751 39. Kanemura, N., Shibata, R., Ohashi, K., Ogawa, H., Hiramatsu-Ito, M., Enomoto, T., Yuasa, D., Ito, M.,
752 Hayakawa, S., Otaka, N., Murohara, T., and Ouchi, N. (2017) C1q/TNF-related protein 1 prevents neointimal
753 formation after arterial injury. *Atherosclerosis* **257**, 138-145
- 754 40. Ogawa, H., Ohashi, K., Ito, M., Shibata, R., Kanemura, N., Yuasa, D., Kambara, T., Matsuo, K., Hayakawa,
755 S., Hiramatsu-Ito, M., Otaka, N., Kawanishi, H., Yamaguchi, S., Enomoto, T., Abe, T., Kaneko, M.,
756 Takefuji, M., Murohara, T., and Ouchi, N. (2019) Adipolin/CTRP12 protects against pathological vascular
757 remodeling through suppression of smooth muscle cell growth and macrophage inflammatory response.
758 *Cardiovasc Res*
- 759 41. Otaka, N., Shibata, R., Ohashi, K., Uemura, Y., Kambara, T., Enomoto, T., Ogawa, H., Ito, M., Kawanishi,
760 H., Maruyama, S., Joki, Y., Fujikawa, Y., Narita, S., Unno, K., Kawamoto, Y., Murate, T., Murohara, T., and
761 Ouchi, N. (2018) Myonectin Is an Exercise-Induced Myokine That Protects the Heart From Ischemia-
762 Reperfusion Injury. *Circ Res* **123**, 1326-1338
- 763 42. Uemura, Y., Shibata, R., Ohashi, K., Enomoto, T., Kambara, T., Yamamoto, T., Ogura, Y., Yuasa, D., Joki,
764 Y., Matsuo, K., Miyabe, M., Kataoka, Y., Murohara, T., and Ouchi, N. (2013) Adipose-derived factor
765 CTRP9 attenuates vascular smooth muscle cell proliferation and neointimal formation. *FASEB J* **27**, 25-33
- 766 43. Yuasa, D., Ohashi, K., Shibata, R., Mizutani, N., Kataoka, Y., Kambara, T., Uemura, Y., Matsuo, K.,
767 Kanemura, N., Hayakawa, S., Hiramatsu-Ito, M., Ito, M., Ogawa, H., Murate, T., Murohara, T., and Ouchi,
768 N. (2016) C1q/TNF-related protein-1 functions to protect against acute ischemic injury in the heart. *FASEB J*
769 **30**, 1065-1075
- 770 44. Sun, Y., Yi, W., Yuan, Y., Lau, W. B., Yi, D., Wang, X., Wang, Y., Su, H., Gao, E., Koch, W. J., and Ma, X.
771 L. (2013) C1q/Tumor Necrosis Factor-Related Protein-9, a Novel Adipocyte-Derived Cytokine, Attenuates
772 Adverse Remodeling in the Ischemic Mouse Heart via Protein Kinase A Activation. *Circulation* **128**, S113-
773 120
- 774 45. Yi, W., Sun, Y., Yuan, Y., Lau, W. B., Zheng, Q., Wang, X., Wang, Y., Shang, X., Gao, E., Koch, W. J., and
775 Ma, X. L. (2012) C1q/tumor necrosis factor-related protein-3, a newly identified adipokine, is a novel
776 antiapoptotic, proangiogenic, and cardioprotective molecule in the ischemic mouse heart. *Circulation* **125**,
777 3159-3169
- 778 46. Han, S., Jeong, A. L., Lee, S., Park, J. S., Buyanravjikh, S., Kang, W., Choi, S., Park, C., Han, J., Son, W. C.,
779 Yoo, K. H., Cheong, J. H., Oh, G. T., Lee, W. Y., Kim, J., Suh, S. H., Lee, S. H., Lim, J. S., Lee, M. S., and
780 Yang, Y. (2018) C1q/TNF- α -Related Protein 1 (CTRP1) Maintains Blood Pressure Under Dehydration
781 Conditions. *Circ Res* **123**, e5-e19
- 782 47. Lee, S. M., Lee, J. W., Kim, I., Woo, D. C., Pack, C. G., Sung, Y. H., Baek, I. J., Jung, C. H., Kim, Y. H.,
783 and Ha, C. H. (2022) Angiogenic adipokine C1q-TNF-related protein 9 ameliorates myocardial infarction via
784 histone deacetylase 7-mediated MEF2 activation. *Sci Adv* **8**, eabq0898
- 785 48. Rodriguez, S., Little, H. C., Daneshpajouhnejad, P., Fenaroli, P., Tan, S. Y., Sarver, D. C., Delannoy, M.,
786 Talbot, C. C., Jr., Jandu, S., Berkowitz, D. E., Pluznick, J. L., Rosenberg, A. Z., and Wong, G. W. (2021)
787 Aging and chronic high-fat feeding negatively affect kidney size, function, and gene expression in CTRP1-
788 deficient mice. *Am J Physiol Regul Integr Comp Physiol* **320**, R19-R35
- 789 49. Rodriguez, S., Little, H. C., Daneshpajouhnejad, P., Shepard, B. D., Tan, S. Y., Wolfe, A., Cheema, M. U.,
790 Jandu, S., Woodward, O. M., Talbot, C. C., Jr., Berkowitz, D. E., Rosenberg, A. Z., Pluznick, J. L., and
791 Wong, G. W. (2020) Late-onset renal hypertrophy and dysfunction in mice lacking CTRP1. *FASEB J* **34**,
792 2657-2676
- 793 50. Kirketerp-Moller, N., Bayarri-Olmos, R., Krogfelt, K. A., and Garred, P. (2020) C1q/TNF-Related Protein 6
794 Is a Pattern Recognition Molecule That Recruits Collectin-11 from the Complement System to Ligands. *J*
795 *Immunol* **204**, 1598-1606
- 796 51. Lahav, R., Haim, Y., Bhandarkar, N. S., Levin, L., Chalifa-Caspi, V., Sarver, D., Sahagun, A., Maixner, N.,
797 Kovesh, B., Wong, G. W., and Rudich, A. (2021) CTRP6 rapidly responds to acute nutritional changes,
798 regulating adipose tissue expansion and inflammation in mice. *Am J Physiol Endocrinol Metab* **321**, E702-
799 E713

- 800 52. Ayyagari, R., Mandal, M. N., Karoukis, A. J., Chen, L., McLaren, N. C., Lichter, M., Wong, D. T.,
801 Hitchcock, P. F., Caruso, R. C., Moroi, S. E., Maumenee, I. H., and Sieving, P. A. (2005) Late-onset macular
802 degeneration and long anterior lens zonules result from a CTRP5 gene mutation. *Invest Ophthalmol Vis Sci*
803 **46**, 3363-3371
- 804 53. Hayward, C., Shu, X., Cideciyan, A. V., Lennon, A., Barran, P., Zarepari, S., Sawyer, L., Hendry, G.,
805 Dhillon, B., Milam, A. H., Luthert, P. J., Swaroop, A., Hastie, N. D., Jacobson, S. G., and Wright, A. F.
806 (2003) Mutation in a short-chain collagen gene, CTRP5, results in extracellular deposit formation in late-
807 onset retinal degeneration: a genetic model for age-related macular degeneration. *Hum Mol Genet* **12**, 2657-
808 2667
- 809 54. Luo, Y., Wu, X., Ma, Z., Tan, W., Wang, L., Na, D., Zhang, G., Yin, A., Huang, H., Xia, D., Zhang, Y., Shi,
810 X., and Wang, L. (2016) Expression of the novel adipokine C1qTNF-related protein 4 (CTRP4) suppresses
811 colitis and colitis-associated colorectal cancer in mice. *Cell Mol Immunol* **13**, 688-699
- 812 55. Youngstrom, D. W., Zondervan, R. L., Doucet, N. R., Acevedo, P. K., Sexton, H. E., Gardner, E. A.,
813 Anderson, J. S., Kushwaha, P., Little, H. C., Rodriguez, S., Riddle, R. C., Kalajzic, I., Wong, G. W., and
814 Hankenson, K. D. (2020) CTRP3 Regulates Endochondral Ossification and Bone Remodeling During
815 Fracture Healing. *J Orthop Res* **38**, 996-1006
- 816 56. Hamoud, N., Tran, V., Aimi, T., Kakegawa, W., Lahaie, S., Thibault, M. P., Pelletier, A., Wong, G. W., Kim,
817 I. S., Kania, A., Yuzaki, M., Bouvier, M., and Cote, J. F. (2018) Spatiotemporal regulation of the GPCR
818 activity of BAI3 by C1qL4 and Stabilin-2 controls myoblast fusion. *Nature communications* **9**, 4470
- 819 57. Cho, Y., Kim, H. S., Kang, D., Kim, H., Lee, N., Yun, J., Kim, Y. J., Lee, K. M., Kim, J. H., Kim, H. R.,
820 Hwang, Y. I., Jo, C. H., and Kim, J. H. (2021) CTRP3 exacerbates tendinopathy by dysregulating tendon
821 stem cell differentiation and altering extracellular matrix composition. *Sci Adv* **7**, eabg6069
- 822 58. Kakegawa, W., Mitakidis, N., Miura, E., Abe, M., Matsuda, K., Takeo, Y. H., Kohda, K., Motohashi, J.,
823 Takahashi, A., Nagao, S., Muramatsu, S., Watanabe, M., Sakimura, K., Aricescu, A. R., and Yuzaki, M.
824 (2015) Anterograde C1ql1 signaling is required in order to determine and maintain a single-winner climbing
825 fiber in the mouse cerebellum. *Neuron* **85**, 316-329
- 826 59. Sigoillot, S. M., Iyer, K., Binda, F., Gonzalez-Calvo, I., Talleur, M., Vodjdani, G., Isope, P., and Selimi, F.
827 (2015) The Secreted Protein C1QL1 and Its Receptor BAI3 Control the Synaptic Connectivity of Excitatory
828 Inputs Converging on Cerebellar Purkinje Cells. *Cell reports* **10**, 820-832
- 829 60. Martinelli, D. C., Chew, K. S., Rohlmann, A., Lum, M. Y., Ressler, S., Hattar, S., Brunger, A. T., Missler, M.,
830 and Sudhof, T. C. (2016) Expression of C1ql3 in Discrete Neuronal Populations Controls Efferent Synapse
831 Numbers and Diverse Behaviors. *Neuron* **91**, 1034-1051
- 832 61. Sarver, D. C., Xu, C., Cheng, Y., Terrillion, C. E., and Wong, G. W. (2021) CTRP4 ablation impairs
833 associative learning and memory. *FASEB J* **35**, e21910
- 834 62. Matsuda, K., Budisantoso, T., Mitakidis, N., Sugaya, Y., Miura, E., Kakegawa, W., Yamasaki, M., Konno,
835 K., Uchigashima, M., Abe, M., Watanabe, I., Kano, M., Watanabe, M., Sakimura, K., Aricescu, A. R., and
836 Yuzaki, M. (2016) Transsynaptic Modulation of Kainate Receptor Functions by C1q-like Proteins. *Neuron*
837 **90**, 752-767
- 838 63. Huggett, S. B., and Stallings, M. C. (2020) Genetic Architecture and Molecular Neuropathology of Human
839 Cocaine Addiction. *J Neurosci* **40**, 5300-5313
- 840 64. Unroe, K. A., Glover, M. E., Shupe, E. A., Feng, N., and Clinton, S. M. (2021) Perinatal SSRI Exposure
841 Disrupts G Protein-coupled Receptor BAI3 in Developing Dentate Gyrus and Adult Emotional Behavior:
842 Relevance to Psychiatric Disorders. *Neuroscience* **471**, 32-50
- 843 65. Iijima, T., Miura, E., Watanabe, M., and Yuzaki, M. (2010) Distinct expression of C1q-like family mRNAs
844 in mouse brain and biochemical characterization of their encoded proteins. *Eur J Neurosci* **31**, 1606-1615
- 845 66. Vishvanath, L., and Gupta, R. K. (2019) Contribution of adipogenesis to healthy adipose tissue expansion in
846 obesity. *J Clin Invest* **129**, 4022-4031
- 847 67. Hotamisligil, G. S. (2006) Inflammation and metabolic disorders. *Nature* **444**, 860-867
- 848 68. Sun, K., Tordjman, J., Clement, K., and Scherer, P. E. (2013) Fibrosis and adipose tissue dysfunction. *Cell*
849 *Metab* **18**, 470-477
- 850 69. Masschelin, P. M., Cox, A. R., Chernis, N., and Hartig, S. M. (2019) The Impact of Oxidative Stress on
851 Adipose Tissue Energy Balance. *Front Physiol* **10**, 1638
- 852 70. Hotamisligil, G. S. (2010) Endoplasmic reticulum stress and the inflammatory basis of metabolic disease.
853 *Cell* **140**, 900-917

- 854 71. Ritchie, M. E., Phipson, B., Wu, D., Hu, Y., Law, C. W., Shi, W., and Smyth, G. K. (2015) limma powers
855 differential expression analyses for RNA-sequencing and microarray studies. *Nucleic Acids Res* **43**, e47
856 72. Delezie, J., Dumont, S., Dardente, H., Oudart, H., Grechez-Cassiau, A., Klosen, P., Teboul, M., Delaunay, F.,
857 Pevet, P., and Challet, E. (2012) The nuclear receptor REV-ERB α is required for the daily balance of
858 carbohydrate and lipid metabolism. *FASEB J* **26**, 3321-3335
859 73. Hand, L. E., Usan, P., Cooper, G. J., Xu, L. Y., Ammori, B., Cunningham, P. S., Aghamohammadzadeh, R.,
860 Soran, H., Greenstein, A., Loudon, A. S., Bechtold, D. A., and Ray, D. W. (2015) Adiponectin induces A20
861 expression in adipose tissue to confer metabolic benefit. *Diabetes* **64**, 128-136
862 74. Hunter, A. L., Pelekanou, C. E., Barron, N. J., Northeast, R. C., Grudzien, M., Adamson, A. D., Downton, P.,
863 Cornfield, T., Cunningham, P. S., Billaud, J. N., Hodson, L., Loudon, A. S., Unwin, R. D., Iqbal, M., Ray, D.
864 W., and Bechtold, D. A. (2021) Adipocyte NR1D1 dictates adipose tissue expansion during obesity. *Elife* **10**
865 75. Xu, J., Lloyd, D. J., Hale, C., Stanislaus, S., Chen, M., Sivits, G., Vonderfecht, S., Hecht, R., Li, Y. S.,
866 Lindberg, R. A., Chen, J. L., Jung, D. Y., Zhang, Z., Ko, H. J., Kim, J. K., and Veniant, M. M. (2009)
867 Fibroblast growth factor 21 reverses hepatic steatosis, increases energy expenditure, and improves insulin
868 sensitivity in diet-induced obese mice. *Diabetes* **58**, 250-259
869 76. Sancar, G., Liu, S., Gasser, E., Alvarez, J. G., Moutos, C., Kim, K., van Zutphen, T., Wang, Y., Huddy, T. F.,
870 Ross, B., Dai, Y., Zepeda, D., Collins, B., Tilley, E., Kolar, M. J., Yu, R. T., Atkins, A. R., van Dijk, T. H.,
871 Saghatelian, A., Jonker, J. W., Downes, M., and Evans, R. M. (2022) FGF1 and insulin control lipolysis by
872 convergent pathways. *Cell Metab* **34**, 171-183 e176
873 77. Zhao, L., Fan, M., Zhao, L., Yun, H., Yang, Y., Wang, C., and Qin, D. (2020) Fibroblast growth factor 1
874 ameliorates adipose tissue inflammation and systemic insulin resistance via enhancing adipocyte
875 mTORC2/Rictor signal. *J Cell Mol Med* **24**, 12813-12825
876 78. Fan, L., Ding, L., Lan, J., Niu, J., He, Y., and Song, L. (2019) Fibroblast Growth Factor-1 Improves Insulin
877 Resistance via Repression of JNK-Mediated Inflammation. *Front Pharmacol* **10**, 1478
878 79. Kong, X., Feng, D., Wang, H., Hong, F., Bertola, A., Wang, F. S., and Gao, B. (2012) Interleukin-22 induces
879 hepatic stellate cell senescence and restricts liver fibrosis in mice. *Hepatology* **56**, 1150-1159
880 80. Yang, L., Zhang, Y., Wang, L., Fan, F., Zhu, L., Li, Z., Ruan, X., Huang, H., Wang, Z., Huang, Z., Huang,
881 Y., Yan, X., and Chen, Y. (2010) Amelioration of high fat diet induced liver lipogenesis and hepatic steatosis
882 by interleukin-22. *J Hepatol* **53**, 339-347
883 81. Wang, X., Ota, N., Manzanillo, P., Kates, L., Zavala-Solorio, J., Eidenschenk, C., Zhang, J., Lesch, J., Lee,
884 W. P., Ross, J., Diehl, L., van Bruggen, N., Kolumam, G., and Ouyang, W. (2014) Interleukin-22 alleviates
885 metabolic disorders and restores mucosal immunity in diabetes. *Nature* **514**, 237-241
886 82. Choi, C. S., Fillmore, J. J., Kim, J. K., Liu, Z. X., Kim, S., Collier, E. F., Kulkarni, A., Distefano, A., Hwang,
887 Y. J., Kahn, M., Chen, Y., Yu, C., Moore, I. K., Reznick, R. M., Higashimori, T., and Shulman, G. I. (2007)
888 Overexpression of uncoupling protein 3 in skeletal muscle protects against fat-induced insulin resistance. *J*
889 *Clin Invest* **117**, 1995-2003
890 83. Fan, L., Sweet, D. R., Prosdocimo, D. A., Vinayachandran, V., Chan, E. R., Zhang, R., Ilkayeva, O., Lu, Y.,
891 Keerthy, K. S., Booth, C. E., Newgard, C. B., and Jain, M. K. (2021) Muscle Kruppel-like factor 15 regulates
892 lipid flux and systemic metabolic homeostasis. *J Clin Invest* **131**
893 84. Consortium, G. T. (2013) The Genotype-Tissue Expression (GTEx) project. *Nat Genet* **45**, 580-585
894 85. Velez, L. M., Van, C., Moore, T., Zhou, Z., Johnson, C., Hevener, A. L., and Seldin, M. M. (2022) Genetic
895 variation of putative myokine signaling is dominated by biological sex and sex hormones. *Elife* **11**
896 86. Sarver, D. C., Xu, C., Velez, L. M., Aja, S., Jaffe, A. E., Seldin, M. M., Reeves, R. H., and Wong, G. W.
897 (2023) Dysregulated systemic metabolism in a Down syndrome mouse model. *Mol Metab* **68**, 101666
898 87. Kloting, N., Fasshauer, M., Dietrich, A., Kovacs, P., Schon, M. R., Kern, M., Stumvoll, M., and Bluher, M.
899 (2010) Insulin-sensitive obesity. *Am J Physiol Endocrinol Metab* **299**, E506-515
900 88. Primeau, V., Coderre, L., Karelis, A. D., Brochu, M., Lavoie, M. E., Messier, V., Sladek, R., and Rabasa-
901 Lhoret, R. (2011) Characterizing the profile of obese patients who are metabolically healthy. *Int J Obes*
902 *(Lond)* **35**, 971-981
903 89. Samocha-Bonet, D., Chisholm, D. J., Tonks, K., Campbell, L. V., and Greenfield, J. R. (2012) Insulin-
904 sensitive obesity in humans - a 'favorable fat' phenotype? *Trends Endocrinol Metab* **23**, 116-124
905 90. Stefan, N., Kantartzis, K., Machann, J., Schick, F., Thamer, C., Rittig, K., Balletshofer, B., Machicao, F.,
906 Fritsche, A., and Haring, H. U. (2008) Identification and characterization of metabolically benign obesity in
907 humans. *Arch Intern Med* **168**, 1609-1616

- 908 91. Calori, G., Lattuada, G., Piemonti, L., Garancini, M. P., Ragona, F., Villa, M., Mannino, S., Crosignani, P.,
909 Bosi, E., Luzi, L., Ruotolo, G., and Perseghin, G. (2011) Prevalence, metabolic features, and prognosis of
910 metabolically healthy obese Italian individuals: the Cremona Study. *Diabetes Care* **34**, 210-215
- 911 92. Aguilar-Salinas, C. A., Garcia, E. G., Robles, L., Riano, D., Ruiz-Gomez, D. G., Garcia-Ulloa, A. C.,
912 Melgarejo, M. A., Zamora, M., Guillen-Pineda, L. E., Mehta, R., Canizales-Quinteros, S., Tusie Luna, M. T.,
913 and Gomez-Perez, F. J. (2008) High adiponectin concentrations are associated with the metabolically healthy
914 obese phenotype. *J Clin Endocrinol Metab* **93**, 4075-4079
- 915 93. Smith, G. I., Mittendorfer, B., and Klein, S. (2019) Metabolically healthy obesity: facts and fantasies. *J Clin*
916 *Invest* **129**, 3978-3989
- 917 94. Pataky, Z., Bobbioni-Harsch, E., and Golay, A. (2010) Open questions about metabolically normal obesity.
918 *Int J Obes (Lond)* **34 Suppl 2**, S18-23
- 919 95. Samuel, V. T., Petersen, K. F., and Shulman, G. I. (2010) Lipid-induced insulin resistance: unravelling the
920 mechanism. *Lancet* **375**, 2267-2277
- 921 96. Cohen, J. C., Horton, J. D., and Hobbs, H. H. (2011) Human fatty liver disease: old questions and new
922 insights. *Science* **332**, 1519-1523
- 923 97. Kim, J. Y., van de Wall, E., Laplante, M., Azzara, A., Trujillo, M. E., Hofmann, S. M., Schraw, T., Durand,
924 J. L., Li, H., Li, G., Jelicks, L. A., Mehler, M. F., Hui, D. Y., Deshaies, Y., Shulman, G. I., Schwartz, G. J.,
925 and Scherer, P. E. (2007) Obesity-associated improvements in metabolic profile through expansion of
926 adipose tissue. *J Clin Invest* **117**, 2621-2637
- 927 98. Hotamisligil, G. S., Johnson, R. S., Distel, R. J., Ellis, R., Papaioannou, V. E., and Spiegelman, B. M. (1996)
928 Uncoupling of obesity from insulin resistance through a targeted mutation in aP2, the adipocyte fatty acid
929 binding protein. *Science* **274**, 1377-1379
- 930 99. Brandon, A. E., Small, L., Nguyen, T. V., Suryana, E., Gong, H., Yassmin, C., Hancock, S. E., Pulpitel, T.,
931 Stonehouse, S., Prescott, L., Kebede, M. A., Yau, B., Quek, L. E., Kowalski, G. M., Bruce, C. R., Turner, N.,
932 and Cooney, G. J. (2022) Insulin sensitivity is preserved in mice made obese by feeding a high starch diet.
933 *Elife* **11**
- 934 100. Kusminski, C. M., Holland, W. L., Sun, K., Park, J., Spurgin, S. B., Lin, Y., Askew, G. R., Simcox, J. A.,
935 McClain, D. A., Li, C., and Scherer, P. E. (2012) MitoNEET-driven alterations in adipocyte mitochondrial
936 activity reveal a crucial adaptive process that preserves insulin sensitivity in obesity. *Nat Med* **18**, 1539-1549
- 937 101. Wang, F., Liu, H., Blanton, W. P., Belkina, A., Lebrasseur, N. K., and Denis, G. V. (2009) Brd2 disruption in
938 mice causes severe obesity without Type 2 diabetes. *Biochem J* **425**, 71-83
- 939 102. Karelis, A. D., Faraj, M., Bastard, J. P., St-Pierre, D. H., Brochu, M., Prud'homme, D., and Rabasa-Lhoret, R.
940 (2005) The metabolically healthy but obese individual presents a favorable inflammation profile. *J Clin*
941 *Endocrinol Metab* **90**, 4145-4150
- 942 103. Sun, K., Kusminski, C. M., and Scherer, P. E. (2011) Adipose tissue remodeling and obesity. *J Clin Invest*
943 **121**, 2094-2101
- 944 104. Shulman, G. I. (2014) Ectopic fat in insulin resistance, dyslipidemia, and cardiometabolic disease. *N Engl J*
945 *Med* **371**, 1131-1141
- 946 105. Virtue, S., and Vidal-Puig, A. (2010) Adipose tissue expandability, lipotoxicity and the Metabolic Syndrome-
947 -an allostatic perspective. *Biochim Biophys Acta* **1801**, 338-349
- 948 106. Samuel, V. T., and Shulman, G. I. (2012) Mechanisms for insulin resistance: common threads and missing
949 links. *Cell* **148**, 852-871
- 950 107. Summers, S. A., Chaurasia, B., and Holland, W. L. (2019) Metabolic Messengers: ceramides. *Nat Metab* **1**,
951 1051-1058
- 952 108. Yang, Y., Smith, D. L., Jr., Keating, K. D., Allison, D. B., and Nagy, T. R. (2014) Variations in body weight,
953 food intake and body composition after long-term high-fat diet feeding in C57BL/6J mice. *Obesity (Silver*
954 *Spring)* **22**, 2147-2155
- 955 109. Rogers, N. H., Perfield, J. W., 2nd, Strissel, K. J., Obin, M. S., and Greenberg, A. S. (2009) Reduced energy
956 expenditure and increased inflammation are early events in the development of ovariectomy-induced obesity.
957 *Endocrinology* **150**, 2161-2168
- 958 110. Hong, J., Stubbins, R. E., Smith, R. R., Harvey, A. E., and Nunez, N. P. (2009) Differential susceptibility to
959 obesity between male, female and ovariectomized female mice. *Nutr J* **8**, 11
- 960 111. Heine, P. A., Taylor, J. A., Iwamoto, G. A., Lubahn, D. B., and Cooke, P. S. (2000) Increased adipose tissue
961 in male and female estrogen receptor-alpha knockout mice. *Proc Natl Acad Sci U S A* **97**, 12729-12734

- 962 112. Bryzgalova, G., Lundholm, L., Portwood, N., Gustafsson, J. A., Khan, A., Efendic, S., and Dahlman-Wright,
963 K. (2008) Mechanisms of antidiabetogenic and body weight-lowering effects of estrogen in high-fat diet-fed
964 mice. *Am J Physiol Endocrinol Metab* **295**, E904-912
- 965 113. Stubbins, R. E., Holcomb, V. B., Hong, J., and Nunez, N. P. (2012) Estrogen modulates abdominal adiposity
966 and protects female mice from obesity and impaired glucose tolerance. *Eur J Nutr* **51**, 861-870
- 967 114. Yonezawa, R., Wada, T., Matsumoto, N., Morita, M., Sawakawa, K., Ishii, Y., Sasahara, M., Tsuneki, H.,
968 Saito, S., and Sasaoka, T. (2012) Central versus peripheral impact of estradiol on the impaired glucose
969 metabolism in ovariectomized mice on a high-fat diet. *Am J Physiol Endocrinol Metab* **303**, E445-456
- 970 115. Mauvais-Jarvis, F., Clegg, D. J., and Hevener, A. L. (2013) The role of estrogens in control of energy balance
971 and glucose homeostasis. *Endocr Rev* **34**, 309-338
- 972 116. Correa, S. M., Newstrom, D. W., Warne, J. P., Flandin, P., Cheung, C. C., Lin-Moore, A. T., Pierce, A. A.,
973 Xu, A. W., Rubenstein, J. L., and Ingraham, H. A. (2015) An estrogen-responsive module in the ventromedial
974 hypothalamus selectively drives sex-specific activity in females. *Cell reports* **10**, 62-74
- 975 117. Butera, P. C. (2010) Estradiol and the control of food intake. *Physiol Behav* **99**, 175-180
- 976 118. Xu, Y., Nedungadi, T. P., Zhu, L., Sobhani, N., Irani, B. G., Davis, K. E., Zhang, X., Zou, F., Gent, L. M.,
977 Hahner, L. D., Khan, S. A., Elias, C. F., Elmquist, J. K., and Clegg, D. J. (2011) Distinct hypothalamic
978 neurons mediate estrogenic effects on energy homeostasis and reproduction. *Cell Metab* **14**, 453-465
- 979 119. Krause, W. C., Rodriguez, R., Gegenhuber, B., Matharu, N., Rodriguez, A. N., Padilla-Roger, A. M., Toma,
980 K., Herber, C. B., Correa, S. M., Duan, X., Ahituv, N., Tollkuhn, J., and Ingraham, H. A. (2021) Oestrogen
981 engages brain MC4R signalling to drive physical activity in female mice. *Nature* **599**, 131-135
- 982 120. Bolliger, M. F., Martinelli, D. C., and Sudhof, T. C. (2011) The cell-adhesion G protein-coupled receptor
983 BAI3 is a high-affinity receptor for C1q-like proteins. *Proc Natl Acad Sci U S A* **108**, 2534-2539
- 984 121. Sticco, M. J., Pena Palomino, P. A., Lukacsovich, D., Thompson, B. L., Foldy, C., Ressler, S., and Martinelli,
985 D. C. (2021) C1QL3 promotes cell-cell adhesion by mediating complex formation between ADGRB3/BAI3
986 and neuronal pentraxins. *FASEB J* **35**, e21194
- 987 122. Wang, J., Miao, Y., Wicklein, R., Sun, Z., Wang, J., Jude, K. M., Fernandes, R. A., Merrill, S. A., Wernig,
988 M., Garcia, K. C., and Sudhof, T. C. (2021) RTN4/NoGo-receptor binding to BAI3 adhesion-GPCRs regulates
989 neuronal development. *Cell* **184**, 5869-5885 e5825
- 990 123. Alsharif, H., Latimer, M. N., Perez, K. C., Alexander, J., Rahman, M. M., Challa, A. K., Kim, J. A.,
991 Ramanadham, S., Young, M., and Bhatnagar, S. (2023) Loss of Brain Angiogenesis Inhibitor-3 (BAI3) G-
992 Protein Coupled Receptor in Mice Regulates Adaptive Thermogenesis by Enhancing Energy Expenditure.
993 *Metabolites* **13**
- 994 124. Shiu, F. H., Wong, J. C., Bhattacharya, D., Kuranaga, Y., Parag, R. R., Alsharif, H. A., Bhatnagar, S., Van
995 Meir, E. G., and Escayg, A. (2023) Generation and initial characterization of mice lacking full-length BAI3
996 (ADGRB3) expression. *Basic Clin Pharmacol Toxicol*
- 997 125. Rodriguez, S., Stewart, A. N., Lei, X., Cao, X., Little, H. C., Fong, V., Sarver, D. C., and Wong, G. W.
998 (2019) PRADC1: a novel metabolic-responsive secretory protein that modulates physical activity and
999 adiposity. *FASEB J* **33**, 14748-14759
- 1000 126. Tschop, M. H., Speakman, J. R., Arch, J. R., Auwerx, J., Bruning, J. C., Chan, L., Eckel, R. H., Farese, R. V.,
1001 Jr., Galgani, J. E., Hambly, C., Herman, M. A., Horvath, T. L., Kahn, B. B., Kozma, S. C., Maratos-Flier, E.,
1002 Muller, T. D., Munzberg, H., Pfluger, P. T., Plum, L., Reitman, M. L., Rahmouni, K., Shulman, G. I.,
1003 Thomas, G., Kahn, C. R., and Ravussin, E. (2012) A guide to analysis of mouse energy metabolism. *Nat*
1004 *Methods* **9**, 57-63
- 1005 127. Schneider, C. A., Rasband, W. S., and Eliceiri, K. W. (2012) NIH Image to ImageJ: 25 years of image
1006 analysis. *Nat Methods* **9**, 671-675
- 1007 128. Bray, N. L., Pimentel, H., Melsted, P., and Pachter, L. (2016) Near-optimal probabilistic RNA-seq
1008 quantification. *Nat Biotechnol* **34**, 525-527
- 1009 129. Kuleshov, M. V., Jones, M. R., Rouillard, A. D., Fernandez, N. F., Duan, Q., Wang, Z., Koplev, S., Jenkins,
1010 S. L., Jagodnik, K. M., Lachmann, A., McDermott, M. G., Monteiro, C. D., Gundersen, G. W., and Ma'ayan,
1011 A. (2016) Enrichr: a comprehensive gene set enrichment analysis web server 2016 update. *Nucleic Acids Res*
1012 **44**, W90-97
- 1013 130. Alliance of Genome Resources, C. (2020) Alliance of Genome Resources Portal: unified model organism
1014 research platform. *Nucleic Acids Res* **48**, D650-D658
- 1015 131. Langfelder, P., and Horvath, S. (2008) WGCNA: an R package for weighted correlation network analysis.
1016 *BMC Bioinformatics* **9**, 559

- 1017 132. Schmittgen, T. D., and Livak, K. J. (2008) Analyzing real-time PCR data by the comparative C(T) method.
1018 *Nat Protoc* **3**, 1101-1108
1019 133. Sievers, F., and Higgins, D. G. (2018) Clustal Omega for making accurate alignments of many protein
1020 sequences. *Protein Sci* **27**, 135-145

1021
1022
1023
1024
1025
1026
1027
1028

FIGURE LEGENDS

1029 **Figure 1. Nutritional regulation of *Ctrp10* expression.** (A) Sequence alignment of full-length human (GenBank #
1030 NP_872334), mouse (NP_997116), chicken (XP_046777733), xenopus frog (XP_031749381), and zebrafish
1031 (XP_001920705) CTRP10/C1qI2 using Clustal-omega (133). Identical amino acids are shaded black and similar
1032 amino acids are shaded grey. Gaps are indicated by dash lines. Signal peptide, collagen domain with characteristic
1033 Gly-X-Y repeats, and the C-terminal globular C1q domain are indicated. (B) *Ctrp10* expression across different
1034 mouse tissues ($n = 10$). (C) Expression of *Ctrp10* across mouse tissues in response to an overnight (16 h) fast or
1035 fasting followed by 2 h refeeding. (D) Expression of *Ctrp10* across mouse tissues in response to a high-fat diet
1036 (HFD) for 12 weeks or a control low-fat diet (LFD). (E) Generation of *Ctrp10* knockout (KO) mice. The entire
1037 protein coding region in exon 1 and 2 of *Ctrp10* was deleted using CRISPR/Cas9 method and confirmed with DNA
1038 sequencing. (F) Wild-type (WT) and KO alleles were confirmed by PCR genotyping. (G) The complete loss of
1039 *Ctrp10* transcript in KO mice was confirmed in mouse cortex, one of the tissues with high *Ctrp10* expression (WT,
1040 $n = 5$; KO, $n = 5$). All expression levels were normalized to β -actin. All data are presented as mean \pm S.E.M. * $P <$
1041 0.05; ** $P < 0.01$; *** $P < 0.001$.

1042

1043 **Figure 2. *Ctrp10*-KO mice fed a low-fat diet have normal body weight and energy balance.** (A-B) Body weight
1044 (A) and body composition analysis (B) of fat mass, % fat mass (relative to body weight), lean mass, and % lean
1045 mass of WT ($n = 17$) and KO ($n = 14$) male mice at 18 weeks of age. (C-D) Body weight (C) and body composition
1046 analysis (D) of fat mass, % fat mass (relative to body weight), lean mass, and % lean mass of WT ($n = 9$) and KO
1047 ($n = 6$) female mice at 13 weeks of age. (E-G) Food intake, physical activity, and energy expenditure (EE) in male
1048 mice at 18 weeks of age across the circadian cycle (light and dark) and metabolic states (ad libitum fed, fasted,

1049 refed) (WT, $n = 11-12$; KO, $n = 10-12$). **(H-J)** Food intake, physical activity, and energy expenditure in female
1050 mice at 13 weeks of age (WT, $n = 9$; KO, $n = 6$). All data are presented as mean \pm S.E.M.

1051

1052 **Figure 3. *Ctrp10*-KO mice fed a low-fat diet have normal fasting-refeeding response and glucose homeostasis.**

1053 (A-B) Overnight fasted and refed blood glucose, serum insulin, triglyceride, cholesterol, non-esterified free fatty
1054 acids (NEFA), and β -hydroxybutyrate levels in male **(A)** and female **(B)** mice. **(C-D)** Blood glucose levels during
1055 glucose tolerance tests (GTT; **C**) and insulin tolerance tests (ITT; **D**) in WT ($n = 17$) and KO ($n = 14$) male mice at
1056 12 weeks of age. **(E-F)** Blood glucose levels during glucose tolerance tests (GTT; **E**) and insulin tolerance tests
1057 (ITT; **F**) in WT ($n = 9$) and KO ($n = 6$) female mice at 20 and 21 weeks of age, respectively. All data are presented
1058 as mean \pm S.E.M. * $P < 0.05$ (two-way ANOVA with Sidak's post hoc tests).

1059

1060 **Figure 4. *Ctrp10*-KO female mice on a low-fat diet develop obesity with age. (A)** Body weights over time of

1061 WT and KO female mice fed a low-fat diet (LFD). **(B)** Representative image of WT and KO female on LFD for 40

1062 weeks. **(C)** Body composition analysis of WT ($n = 9$) and KO ($n = 6$) female mice fed a LFD. **(D)** Representative

1063 H&E stained histology of gonadal white adipose tissue (gWAT) and the quantification of adipocyte cell size ($n = 6$

1064 per genotype). Scale bar = 100 μ M. **(E)** Representative H&E stained histology of inguinal white adipose tissue

1065 (iWAT) and the quantification of adipocyte cell size ($n = 6$ per genotype). Scale bar = 100 μ M. **(F)** 24-hr food

1066 intake data measured manually. **(G)** Fecal frequency, fecal weight, and fecal energy over a 24 hr period. **(H)** Deep

1067 colon temperature measured at the light and dark cycle. **(I-K)** Food intake, physical activity, and energy

1068 expenditure in female mice across the circadian cycle (light and dark) and metabolic states (ad libitum fed, fasted,

1069 refed) (WT, $n = 9$; KO, $n = 6$). Indirect calorimetry analysis was performed after female mice were on LFD for 30

1070 weeks. **(L)** Overnight (16-hr) fasted blood glucose, serum insulin, triglyceride, cholesterol, non-esterified free fatty

1071 acids, and β -hydroxybutyrate levels. **(M)** Very-low density lipoprotein-triglyceride (VLDL-TG) and high-density

1072 lipoprotein-cholesterol (HDL-cholesterol) analysis by FPLC of pooled ($n = 6-7$ per genotype) mouse sera. **(N)**

1073 Blood glucose levels during glucose tolerance tests (GTT). **(O)** Blood glucose levels during insulin tolerance tests

1074 (ITT). GTT and ITT were performed when the female mice reached 28 and 29 weeks of age, respectively. WT, $n =$

1075 9; KO, $n = 6$.

1076

1077 **Figure 5. Sexually dimorphic response of *Ctrp10*-KO mice to an obesogenic diet. (A)** Body weights over time
1078 of WT and KO male mice fed a high-fat diet (HFD). **(B)** Body composition analysis of WT ($n = 17$) and KO ($n =$
1079 14) male mice fed a HFD for 9 weeks. **(C-E)** Food intake, physical activity, and energy expenditure in male mice
1080 across the circadian cycle (light and dark) and metabolic states (*ad libitum* fed, fasted, refed) (WT, $n = 11$; KO, $n =$
1081 11). Indirect calorimetry analysis was performed after male mice were on HFD for 10 weeks. **(F)** Body weights
1082 over time of WT and KO female mice fed a high-fat diet. **(G)** Representative image of WT and KO female mice
1083 after 13 weeks of high-fat feeding. **(H)** Body composition analysis of WT ($n = 17$) and KO ($n = 13$) female mice on
1084 HFD for 6 weeks. **(I-K)** Food intake, physical activity, and energy expenditure in female mice (WT, $n = 11-12$;
1085 KO, $n = 12$) across the circadian cycle (light and dark) and metabolic states (*ad libitum* fed, fasted, refed). Indirect
1086 calorimetry analysis was performed after female mice were on HFD for 6 weeks. **(L)** ANCOVA analysis of energy
1087 expenditure using body weight as a covariate. **(M)** Respiratory exchange ratio (RER). All data are presented as
1088 mean \pm S.E.M. * $P < 0.05$; ** $P < 0.01$; *** $P < 0.001$; **** $P < 0.0001$

1089
1090 **Figure 6. *Ctrp10*-KO mice on a high-fat diet have normal glucose and insulin tolerance. (A-B)** Overnight
1091 fasted and refed blood glucose, serum insulin, triglyceride, cholesterol, non-esterified free fatty acids (NEFA), and
1092 β -hydroxybutyrate levels in male **(A)** and female **(B)** mice fed a HFD for 10 weeks. **(C-D)** Blood glucose levels
1093 during glucose tolerance tests (GTT; **C**) and insulin tolerance tests (ITT; **D**) in WT ($n = 17$) and KO ($n = 14$) male
1094 mice fed a HFD for 10 weeks. **(E-F)** Blood glucose levels during glucose tolerance tests (GTT; **E**) and insulin
1095 tolerance tests (ITT; **F**) in WT ($n = 16$) and KO ($n = 12$) female mice fed a HFD for 8 weeks. **(G)** VLDL-TG and
1096 HDL-cholesterol analysis by FPLC of pooled female mouse sera. All data are presented as mean \pm S.E.M. ** $P <$
1097 0.01 ; *** $P < 0.001$; **** $P < 0.0001$ (two-way ANOVA with Sidak's post hoc tests for fasted/refed data).

1098
1099 **Figure 7. *Ctrp10*-KO female mice fed a HFD do not develop adipose tissue dysfunction and fatty liver. (A)**
1100 Representative images of dissected gonadal white adipose tissue (gWAT) and the quantification of gWAT weight
1101 in WT ($n = 15$) and KO ($n = 12$) female mice fed a HFD for 14 weeks. **(B)** Representative H&E stained histological
1102 sections of gWAT and the quantification of adipocyte cell size ($n = 7$ per genotype). Scale bar = 100 μ M. **(C)**
1103 Representative images of dissected inguinal white adipose tissue (iWAT) and the quantification of iWAT weight in
1104 WT ($n = 15$) and KO ($n = 12$) female mice. **(D)** Representative H&E stained histological sections of iWAT and the

1105 quantification of adipocyte cell size ($n = 7$ per genotype). Scale bar = 100 μ M. **(E)** Expression of genes associated
1106 with inflammation, fibrosis, ER and oxidative stress in gWAT and iWAT of WT ($n = 6$) and KO ($n = 6$) female
1107 mice fed a HFD for 14 weeks. Gene expression data were obtained from RNA-seq. **(F-G)** Quantification of
1108 hydroxyproline (marker of fibrosis) and malondialdehyde (MDA; marker of oxidative stress) in gWAT and iWAT.
1109 WT, $n = 15$; KO, $n = 11$. **(H)** Representative images of dissected liver and the quantification of liver weight in WT
1110 ($n = 15$) and KO ($n = 12$) female mice. **(I)** Representative H&E stained histological sections of liver and the
1111 quantification of hepatic lipid content (% lipid area; $n = 7$ per genotype). Scale bar = 100 μ M. **(J)** Hepatic
1112 expression of genes associated with inflammation, fibrosis, ER and oxidative stress, lipid synthesis, and lipid
1113 catabolism in WT and KO female mice. Gene expression data were obtained from RNA-seq. **(K-L)** Quantification
1114 of hydroxyproline (marker of fibrosis) and malondialdehyde (MDA; marker of oxidative stress) in liver. WT, $n =$
1115 15; KO, $n = 11$. All data are presented as mean \pm S.E.M. * $P < 0.05$; ** $P < 0.01$.

1116

1117 **Figure 8. Transcriptomic analysis of liver, adipose tissue, and skeletal muscle of female *Ctrp10* KO mice fed a**
1118 **high-fat diet. (A-D)** Cropped volcano plot views of all differentially expressed genes (DEGs, Log₂(Fold Change)
1119 >1 or <-1 with a p -value <0.05) of the liver, gonadal white adipose tissue (gWAT), inguinal WAT (iWAT), or
1120 skeletal muscle (gastrocnemius). **(E)** Overlap analysis of tissue DEGs showing (top panel) expression unique to
1121 gonadal white adipose tissue (gW), inguinal white adipose tissue (iW), liver (L), or skeletal muscle (M). Percent
1122 (%) represents percent DEGs unique to each tissue. Bottom panel show DEGs shared across multiple tissues, with
1123 all the shared DEGs listed. **(F)** Enrichr analysis (129) of biological pathways and processes significantly ($p < 0.01$)
1124 affected across the CTRP10 deficient female mice. Top pathways and processes derived from Gene Ontology (GO),
1125 Reactome (R-HAS), WikiPathway human (WP), and mammalian phenotype (MP). All up- or down-regulated
1126 DEGs across all tissues were used for analysis. The tissues contributing to the highest ranked pathways and
1127 processes are specified. $n = 6$ KO and 6 WT for RNA-seq experiments.

1128

1129 **Figure 9. Loss of CTRP10 induces significant and wide-spread alterations in the expression of key**
1130 **transcription factors, secreted protein, membrane receptors, and metabolism-associated genes. (A-D)**
1131 Selected genes from the DEG list of each tissue organized based on gene type (genes encoding transcription factors,

1132 secreted proteins, receptors, and proteins involved in metabolism) and ranked from highest to lowest row z-score. n
1133 = 6 per genotype
1134
1135 **Figure 10. GTEx genetic co-correlation of mouse differentially expressed gene (DEG) orthologues. (A-B)**
1136 Heatmaps showing biweight midcorrelation (bicor) coefficient among human tissue DEG orthologues in females
1137 (A) and males (B) in GTEx. Y-axis color indicates tissue of origin, P -value based on students' regression P -value.
1138 (C) T-tests between correlation coefficient in males and females among all DEG orthologue gene pairs for
1139 subcutaneous (SubQ) adipose tissue, visceral (visc) adipose tissue, liver, and skeletal muscle. (D) the same as in C,
1140 except comparisons are shown for all gene-gene pairs between tissues. For example, the top left graph compared
1141 the connectivity of males (blue color) vs females (green color) for correlation between subcutaneous (SubQ) and
1142 visceral (Visc) adipose tissue DEG orthologues.

A

Signal peptide

Human	1	MALGLLI AVPLLLQA- APRGAAHYE M MGT CRM CDPYI AAP GGE PPGAKA QPPGP- STAAL EVMQDLS ANPP PPF I QGPKGDP GR
Mouse	1	MALGLLI AVPLLLQA- APPGAAHYE M MGT CRM CDPYS VAPAGGPA GAKA P PGP- STAAL EVMQDLS ANPP PPF I QGPKGDP GR
Chicken	1	MAVALLVAVPLLLQA PAES GAHYE M MGT CRM CDPYS GAR----- PPGPG STAAL EAL QDL GANPP PPF A QGPKGDP GR
Xenopus	1	MLLVLVV I P L L L V - - L P P P G E G H Y E M M G T C R M C D P Y S G H P - - - - - S T A I G E A L Q D L S G - A P P P P F I Q G P K G D P G R
Zebrafish	1	MI AALV I A L P L L L - - - R T P A A H Y E M M G T C R M C D P Y N P K P - - - - - S A T A L E V M Q D L S A - I P P A F A Q G T R G E P G R

Collagen domain

Human	84	PGKPGPRGPPGEPGPPGPRGPPGEGK GDSGRPGLPGLQLTAGTASGVGVVGGGAGVGGDSEGEVTSALSAIFSGPKI AFYVGLKSP
Mouse	84	PGKPGPRGPPGEPGPPGPRGPPGEGK GDSGRPGLPGLQLTTSAAAGGVGVVSGGTGGGDT EGEVTSALSAAFSGPKI AFYVGLKSP
Chicken	76	PGKPGPRGPPGEPGPPGPRGPPGERGDAGKPLPGLPLAGAG-----GGGSGGAAAGGEEAAGGLSAAFGGPRI AFYVGLKSP
Xenopus	68	PGKPGARGPPGEPGPPGPRGPPGERGEPGKAGI PGLGTS-----MPGAVSATLPSPRI AFYVGLKSP
Zebrafish	67	PGKPGPRGPPGEPGPPGPRGPPGDSGRPGFTGVAS---GT-----ARTETGDVGPALGNAKI AFYVGLKNP

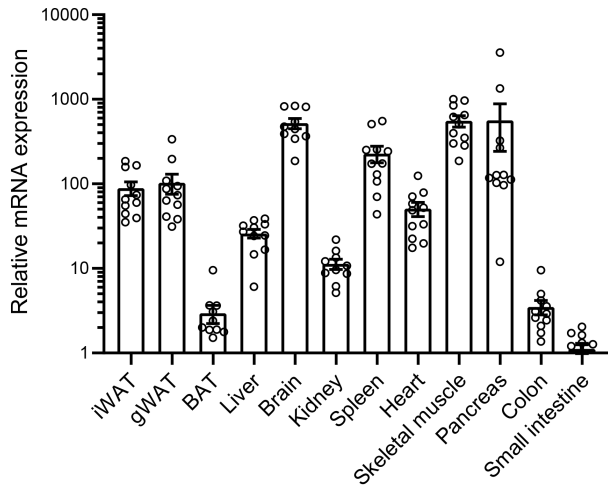
C1q domain

Human	169	HEGYEVLKFDVVVTNLGNHYDPTTGKFSICQVRGIYFFTYHILMRGGDGTSMVADLCKNGQVRASAI AQDADQNYDYASNSVVLHL
Mouse	169	HEGYEVLKFDVVVTNLGNHYDPTTGKFSICQVRGIYFFTYHILMRGGDGTSMVADLCKNGQVRASAI AQDADQNYDYASNSVVLHL
Chicken	154	HEGYEVLKFDVVVTNLGNHYDPTASGKFTCQVRGIYFFTYHILMRGGDGTSMVADLCKNGQVRASAI AQDADQNYDYASNSVVLHL
Xenopus	130	HEGYELKFDVVVTNLGNHYDPTTGKFTCQVPIYFFTYHILMRGGDGTSMVADLCKNGQVRASAI AQDADQNYDYASNSVVLHL
Zebrafish	130	HEGYEVLKFDVVVTNLGNHYDPTTGKFTCQVSGIYFFTYHVLMRGGDGTSMVADLCKNGQVRASAI AQDADQNYDYASNSVVLHL

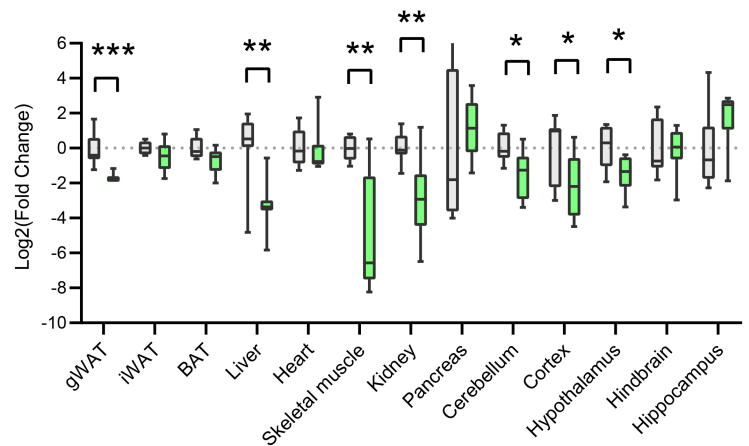
Human	254	DSGDEVYVKLDGGKAHGGNNNKYSTFSGFLLYPD
Mouse	254	DSGDEVYVKLDGGKAHGGNNNKYSTFSGFLLYPD
Chicken	239	DSGDEVYVKLDGGKAHGGNNNKYSTFSGFLLYPD
Xenopus	215	DSGDEVYVKLDGGKAHGGNNNKYSTFSGFLLYPD
Zebrafish	215	DSGDEVYVKLDGGKAHGGNNNKYSTFSGFLLYPD

□ Fasted (n = 7)
■ Refed (n = 8)

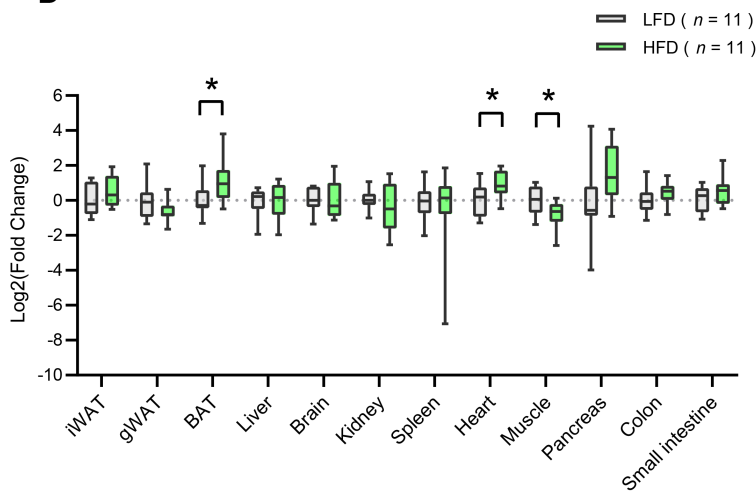
B



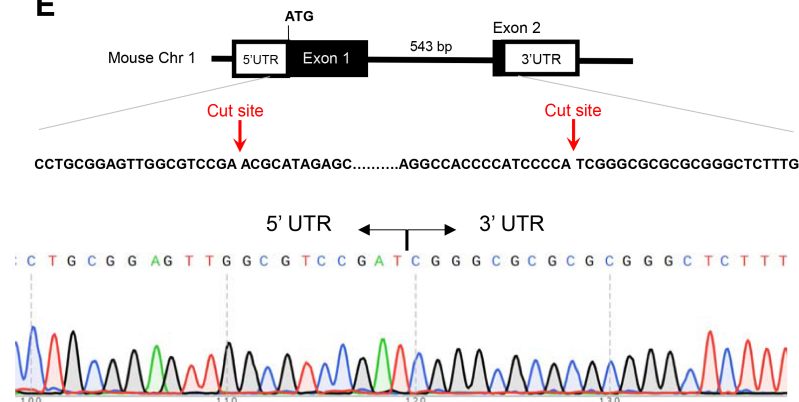
C



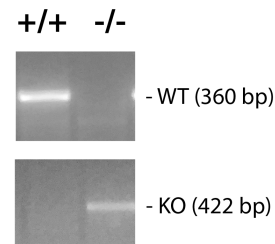
D



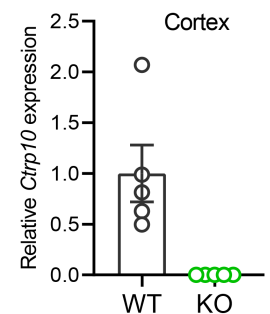
E

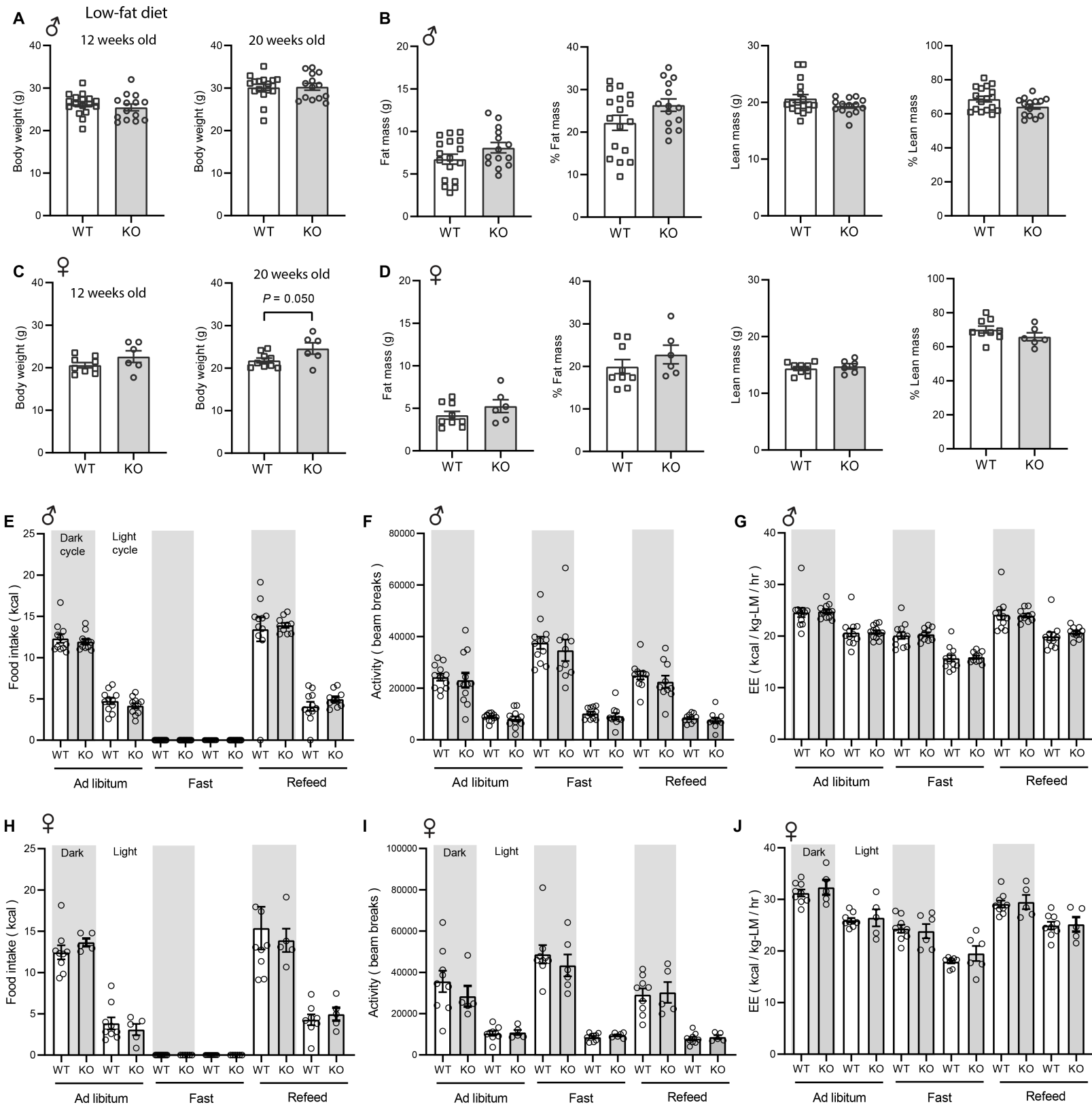


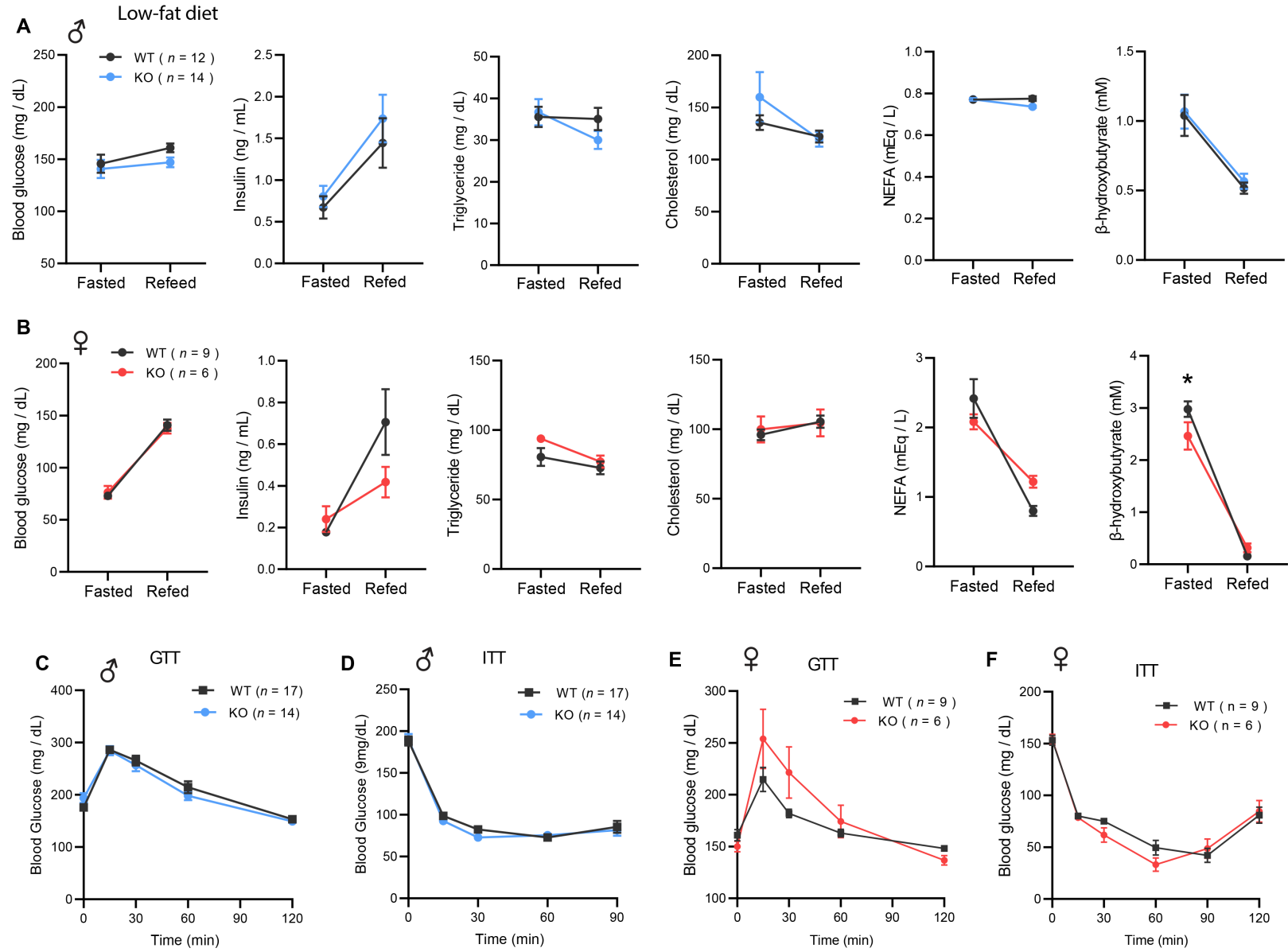
F

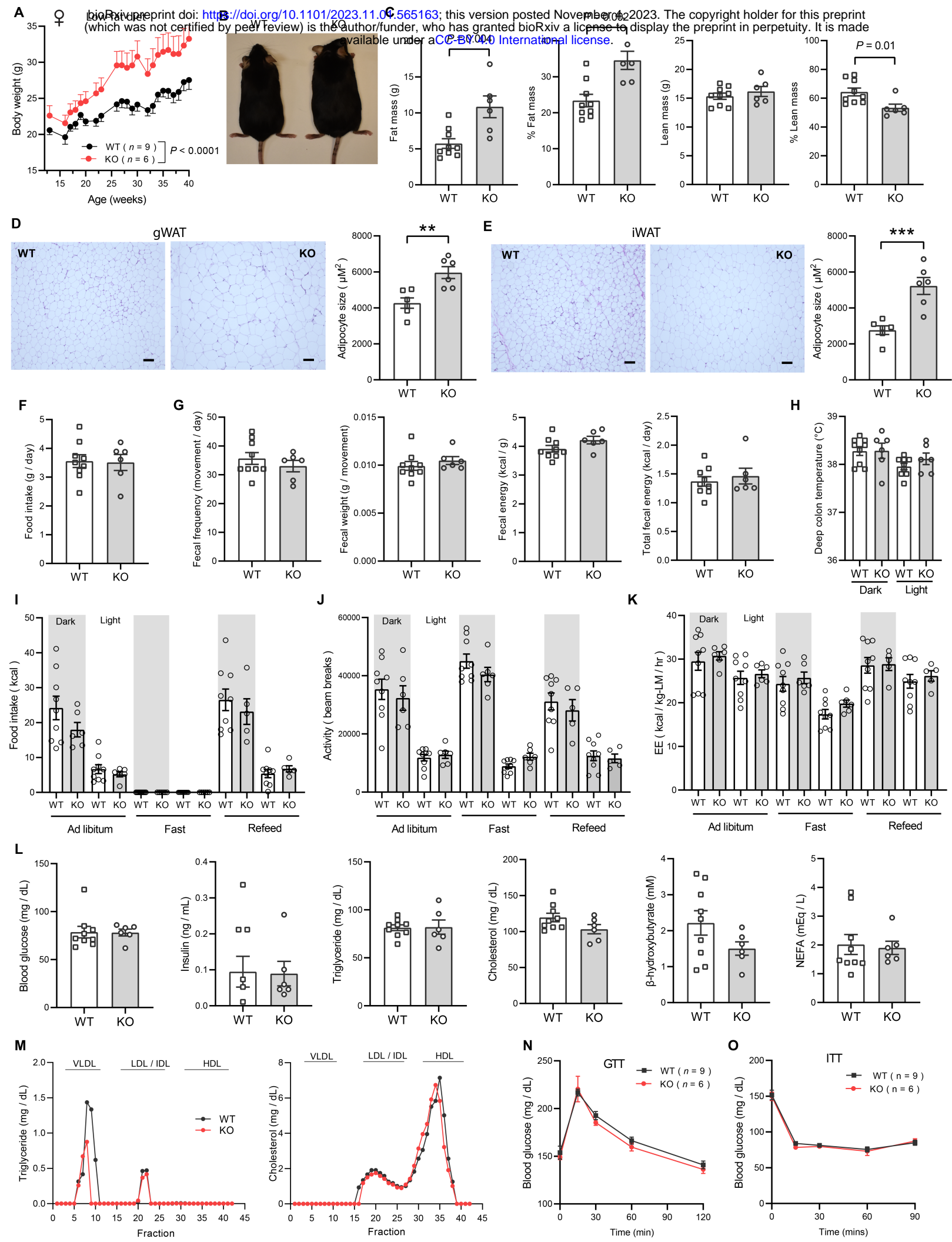


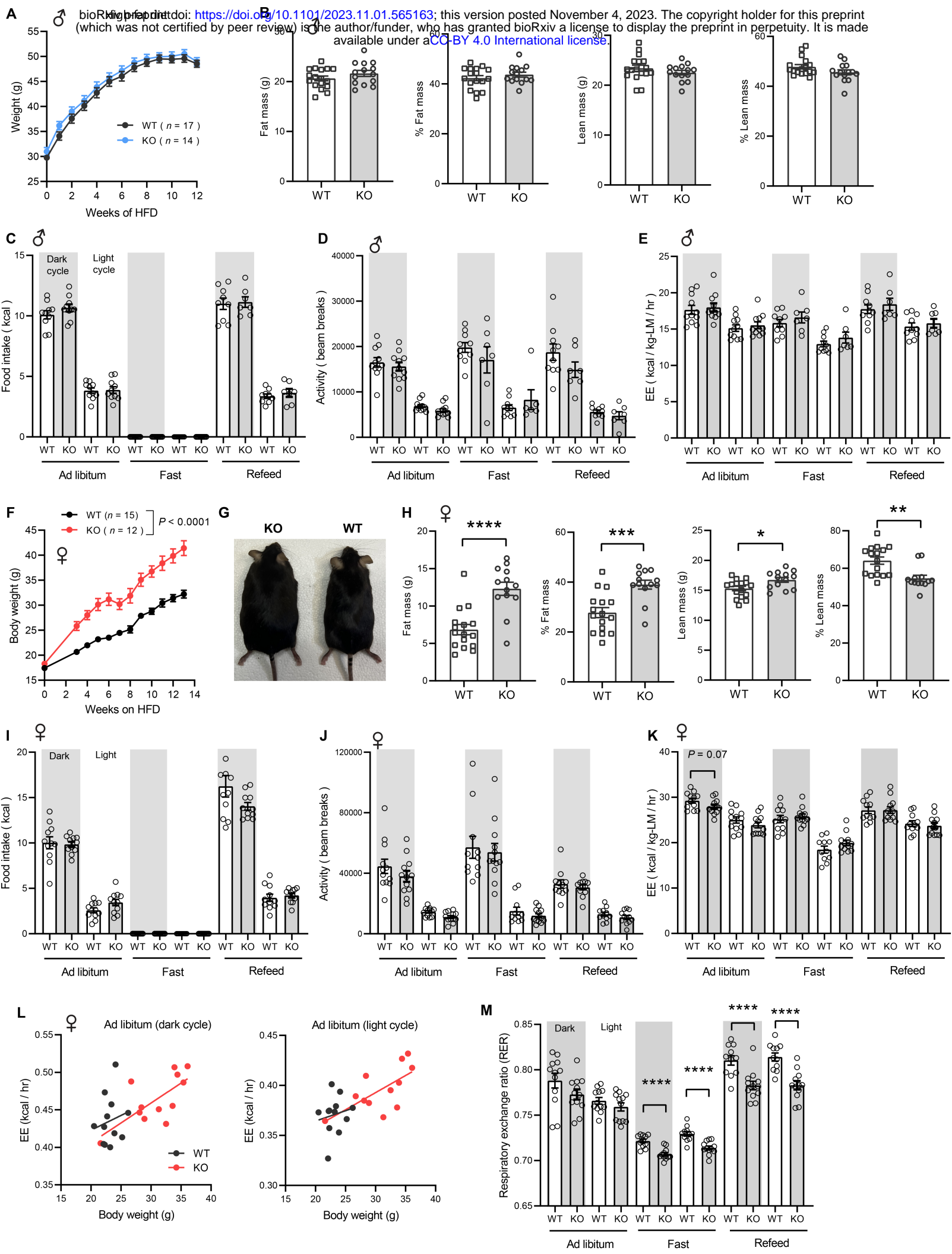
G

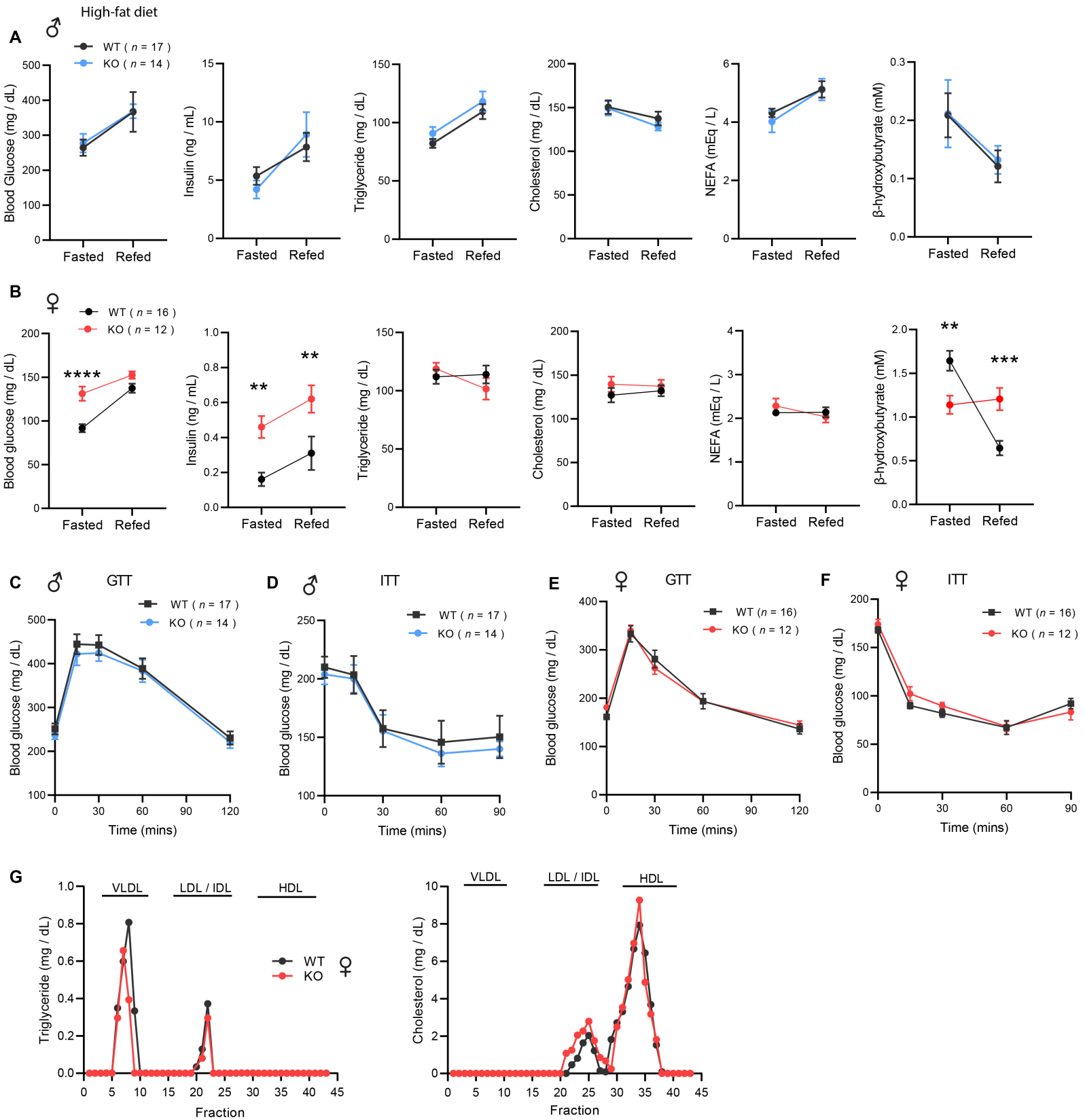


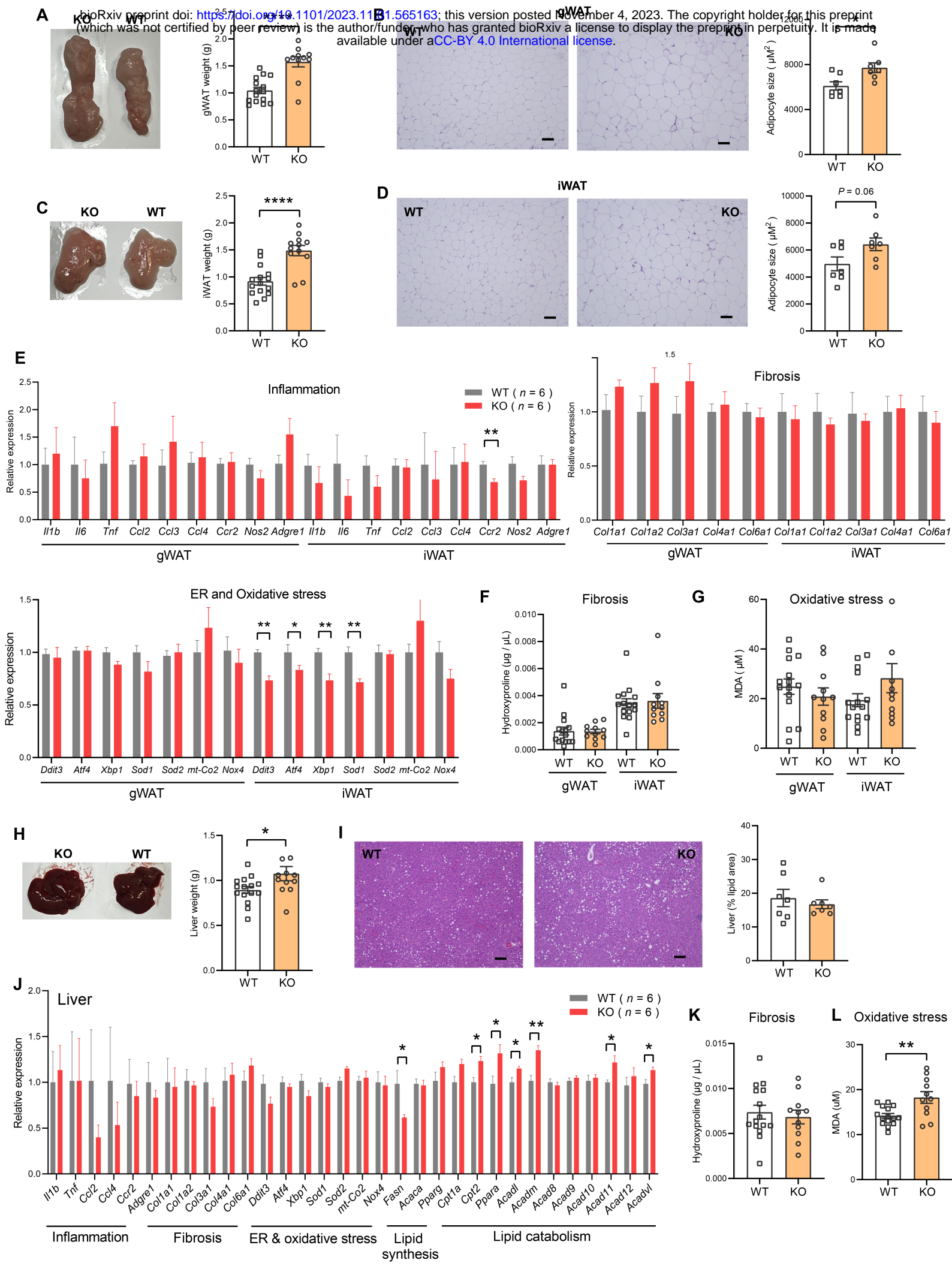


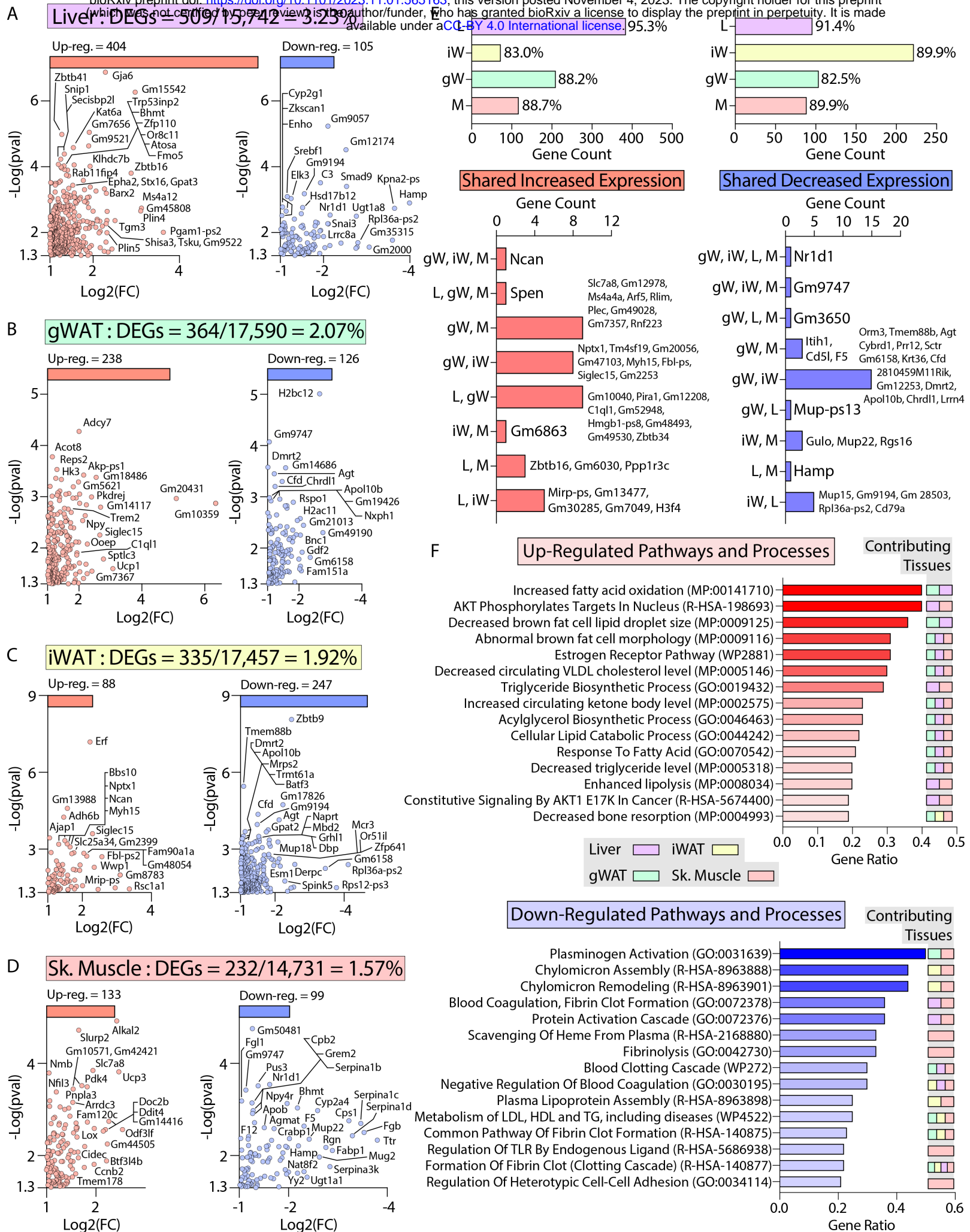


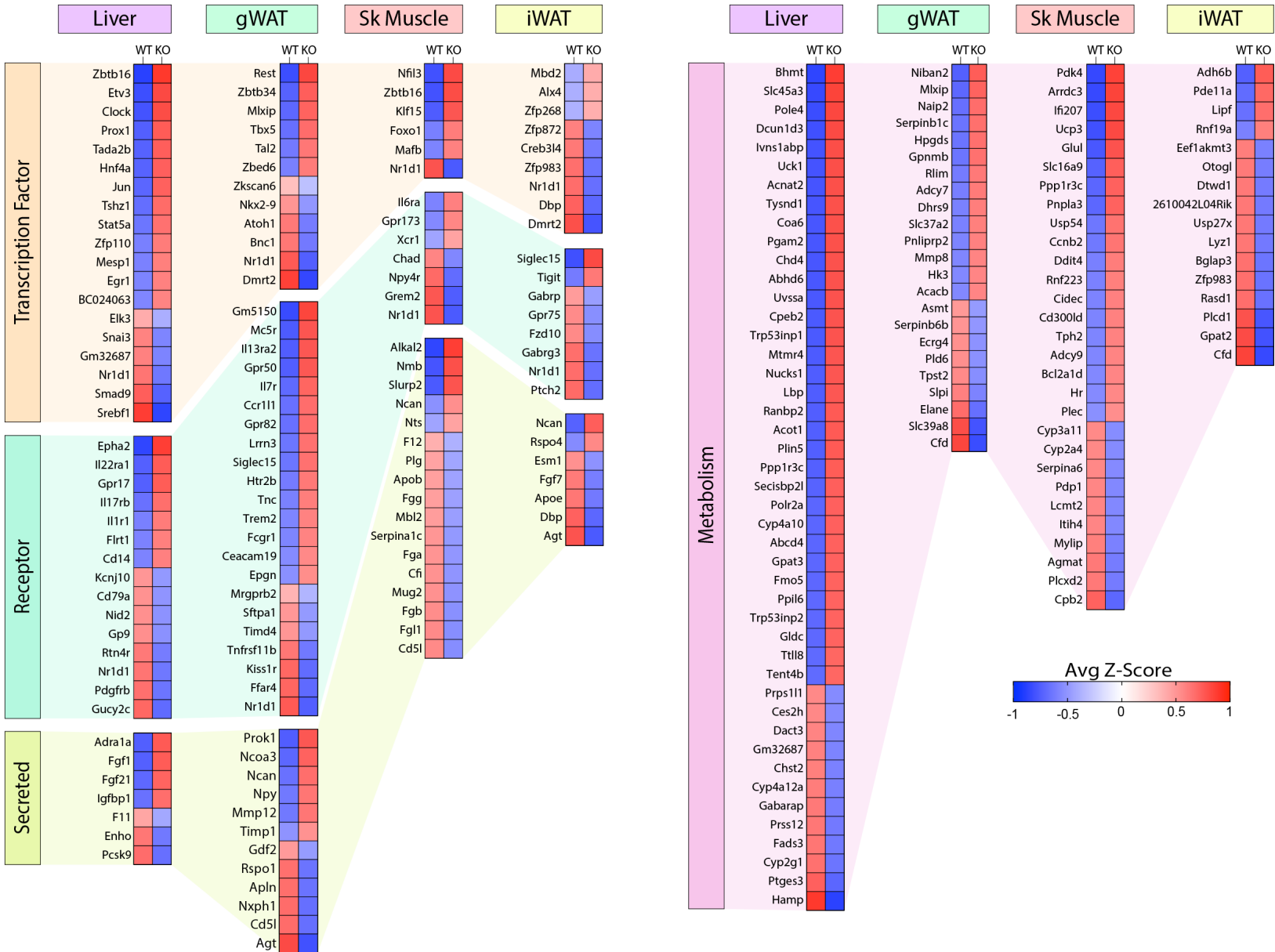








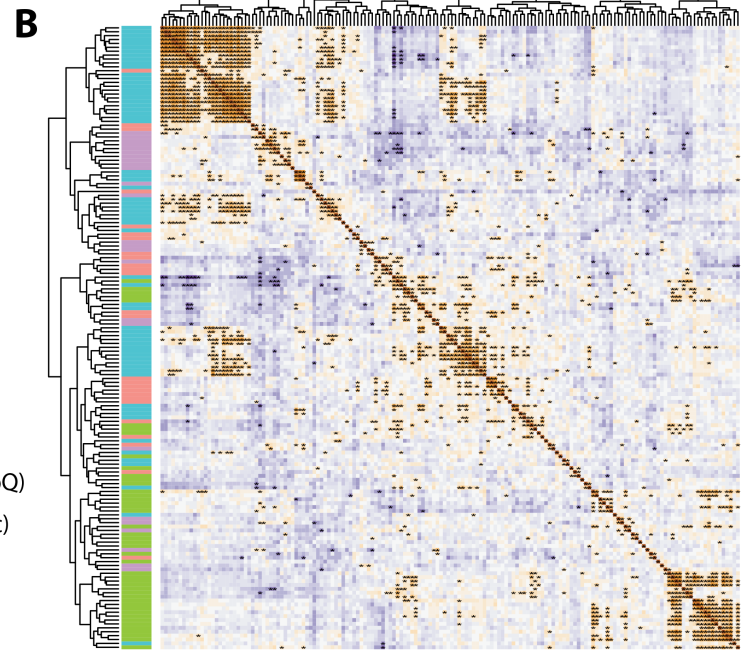
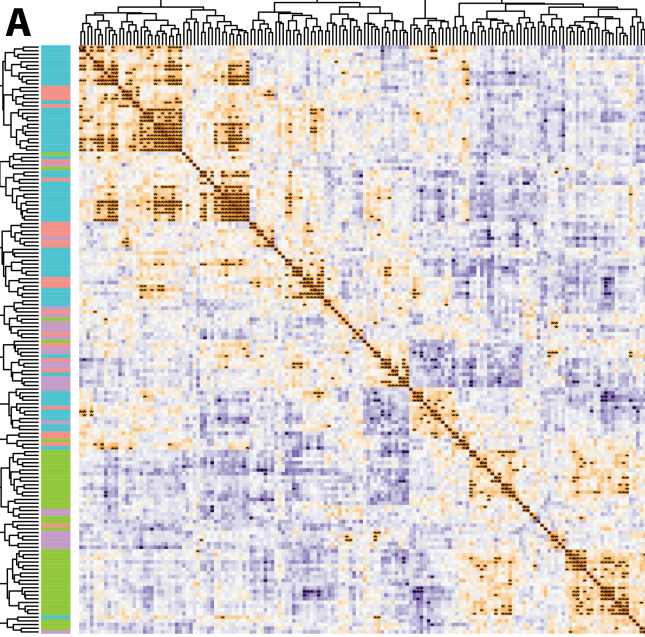




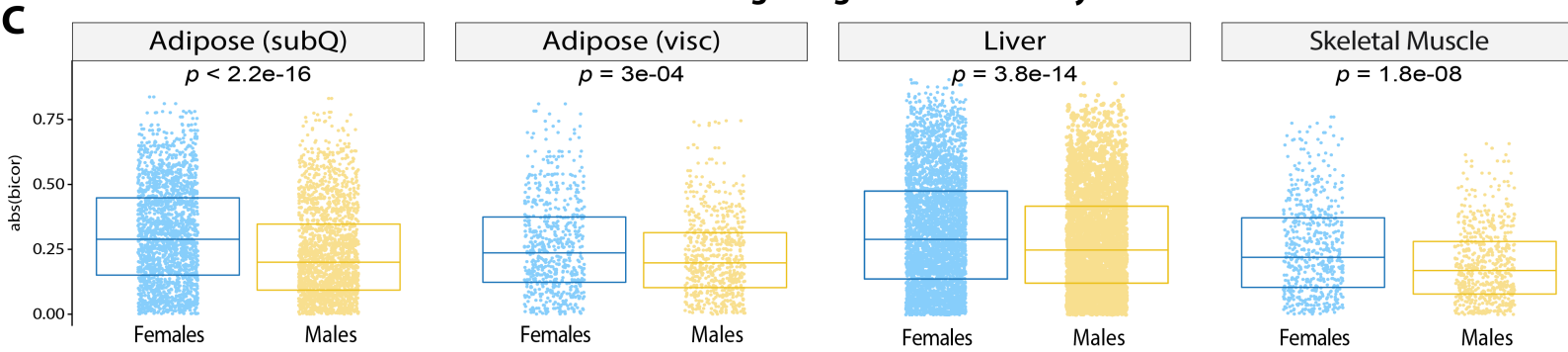
Females

Human DEG Correlation (GTEx)

Males



Within tissue gene-gene connectivity



Across tissue gene-gene connectivity

